Infection, Genetics and Evolution 139 (2026) 105923

Contents lists available at ScienceDirect

Infection, Genetics and Evolution

journal homepage: www.elsevier.com/locate/meegid

Research paper

The role of environmental contamination in the dynamics of HIV–TB co-infection with control strategies: Caputo fractional-order approach

Dickson D. Luambano [a,b,*], Mussa A. Stephano [c], Maranya M. Mayengo [a]

[a] Department of Applied Mathematics, The Nelson Mandela African Institution of Science and Technology, P.O. Box 447, Arusha, Tanzania
[b] Department of Computer Science and Mathematics, Institute of Accountancy Arusha, P.O. Box 2798, Arusha, Tanzania
[c] Department of Mathematics, Physics and Informatics, Mkwawa University College of Education, P.O. Box 2513, Iringa, Tanzania

ARTICLE INFO

Keywords:
HIV–TB co-infection
Fractional-order model
Environmental TB transmission
Ulam–Hyers stability
Control strategies
Sensitivity analysis

ABSTRACT

This study investigates the effectiveness of integrated environmental and medical interventions in controlling HIV–TB co-infection. A Caputo fractional-order modeling framework is developed to capture memory and nonlocal effects inherent in chronic infections, while explicitly incorporating environmental reservoirs of Mycobacterium tuberculosis as an additional transmission pathway. The mathematical well-posedness of the model is established through existence, uniqueness, positivity, boundedness, and Ulam–Hyers stability analysis. Numerical solutions are obtained using an Adams–Bashforth–Moulton predictor–corrector scheme, and unknown parameters are calibrated using World Health Organization HIV–TB co-infection data from Tanzania spanning 2000–2023. The estimated fractional order is $p = 0.982$, indicating strong memory effects that reflect the cumulative impact of past infection history, delayed immune responses, prolonged treatment effects, and persistent environmental contamination characteristic of HIV–TB co-infection dynamics. Model validation using an independent dataset from Kenya (2000–2023) demonstrates the robustness and geographic transferability of the proposed framework. Sensitivity analysis identifies key epidemiological parameters governing transmission and control, emphasizing the joint importance of clinical treatment and environmental sanitation. A comparative analysis between the fractional-order model ($p = 0.982$) and the classical integer-order model ($p = 1$) reveals that the fractional formulation provides an improved fit to observed data and captures long-term disease dynamics more accurately, particularly in reproducing persistent infection trends. Overall, the results show that coordinated medical interventions combined with environmental control substantially reduce HIV–TB co-infection prevalence, underscoring the necessity of integrated, multi sectoral strategies for sustainable disease management in high-burden settings.

1. Introduction

Human Immunodeficiency Virus (HIV) and tuberculosis (TB) continue to impose a severe global health burden, with their combined impact being most pronounced in sub-Saharan Africa (Adeyemo et al., 2023; Ayele et al., 2024a; Obeagu and Obeagu, 2023). HIV compromises host immunity by progressively depleting $CD4^+$ T cells, thereby increasing vulnerability to a wide range of opportunistic infections (Adeyemo et al., 2023; Zahli et al., 2024). Among these, TB remains the most prevalent and deadly, particularly in settings with limited access to early diagnosis and sustained treatment (Singh et al., 2016; Olaniyi et al., 2013; West and Thompson, 1997; Abdullahi et al., 2019). Despite notable progress in antiretroviral therapy and TB chemotherapy, co-infection remains a leading cause of morbidity and mortality in many low- and middle-income countries.

The mutually reinforcing interaction between HIV and TB significantly accelerates disease progression, increases mortality, and complicates treatment outcomes (World Health Organization (WHO), 2023; Endalamaw et al., 2019; Gelaw et al., 2019; Mchunu et al., 2016; Pathmanathan et al., 2018). HIV weakens the immune system, thereby enhancing susceptibility to TB infection and reactivation, while TB infection increases HIV viral replication and hastens the onset of Acquired Immunodeficiency Syndrome (AIDS) (Singh et al., 2016; Olaniyi et al., 2013; West and Thompson, 1997; Abdullahi et al., 2019). These feedback mechanisms complicate clinical management and undermine the effectiveness of single-disease interventions. As a result, HIV–TB co-infection poses unique challenges that cannot be adequately addressed by treating each disease in isolation.

* Corresponding author at: Department of Applied Mathematics, The Nelson Mandela African Institution of Science and Technology, P.O. Box 447, Arusha, Tanzania.
E-mail address: luambanod@nm-aist.ac.tz (D.D. Luambano).

https://doi.org/10.1016/j.meegid.2026.105923
Received 14 January 2026; Received in revised form 16 February 2026; Accepted 5 March 2026
Available online 6 March 2026

The divergent clinical courses and therapeutic strategies for HIV and tuberculosis (TB) necessitate integrated treatment approaches for co-infected individuals (Ayele et al., 2024a; Mallela et al., 2016). Standard practice mandates prompt initiation of TB treatment, given its effective and finite regimen (Ayele et al., 2024a). However, the timing of ART initiation presents a therapeutic dilemma. Initiating ART concurrently with or shortly after TB treatment may precipitate Immune Reconstitution Inflammatory Syndrome (IRIS) (Ayele et al., 2024a; Mallela et al., 2016), a condition characterized by worsening TB symptoms and severe complications that can lead to treatment interruption. Alternatively, postponing ART until TB treatment completion elevates the risks of HIV-related mortality and onward transmission (Ayele et al., 2024a; Mallela et al., 2016). Therefore, determining the ideal combination treatment protocol is a crucial unmet need in co-infection management.

Recent developments in disease modeling show a shift toward fractional and fractal–fractional systems, which better represent biological processes such as memory effects and complex nonlinear interactions. These approaches are often enhanced by artificial intelligence and neural networks, improving analysis, numerical approximation, and predictive accuracy. Applications of such hybrid frameworks include modeling chronic myeloid leukemia (Shah et al., 2024), predicting viral eye infections (Shah et al., 2025a), analyzing epidemic models (Shah et al., 2025b), solving complex fractional integro-differential equations (Sher et al., 2025), and even modeling psychological disorders (Alqudah et al., 2026). These hybrid approaches highlight the growing importance of combining mechanistic fractional-order models with advanced computational techniques, reinforcing the relevance of the present fractional HIV–TB framework. Motivated by these advances, this study adopts a fractional-order modeling framework to better capture the transmission dynamics of HIV–TB co-infection.

Mathematical modeling has long been essential for understanding HIV–TB transmission and evaluating intervention strategies. Classical integer-order models provide valuable insights into disease dynamics and control strategies (Ayele et al., 2024a; Adesola et al., 2024; Awoke and Kassa, 2018; Seidu et al., 2023; Teklu et al., 2023), but they often fail to capture long-term memory effects, host variability, and delays associated with treatment adherence or environmental persistence. To address these limitations, fractional-order models, particularly those based on the Caputo derivative, have been increasingly adopted in epidemiological studies (Kumar et al., 2021). These models naturally incorporate memory effects and nonlocal dynamics, which are especially relevant for chronic infections such as HIV and TB. The Caputo derivative also allows for physically meaningful initial conditions, making it well-suited for realistic epidemiological modeling (Lusekelo et al., 2023).

Recent studies have applied Caputo fractional-order frameworks to HIV-only, TB-only, and HIV–TB co-infection models (Farman et al., 2020; Aggarwal and Raj, 2021; Devi et al., 2025; Gemeda et al., 2025; Raza et al., 2025). Fractional-order operators improve model fidelity by capturing nonlocal temporal effects, demonstrating better agreement with epidemiological data and enhanced stability properties compared to integer-order counterparts (Khan et al., 2021; Kumar et al., 2024, 2023). For instance, Farman et al. (2020) and Aggarwal and Raj (2021) showed that fractional derivatives significantly influence system dynamics, revealing disease-control pathways that classical models might overlook. Further work by Devi et al. (2025) and Gemeda et al. (2025) highlighted the utility of fractional-order differential equations in optimal control design, demonstrating that integrated strategies can nearly eliminate infections under sufficient compliance. Similarly, Raza et al. (2025) emphasized the combined effect of HIV prevention and TB treatment, illustrating the advantages of fractional modeling in co-infection control.

Nonetheless, most existing models either neglect the role of environmental TB reservoirs or simplify environmental transmission, despite evidence that contaminated environments contribute significantly to TB persistence, particularly in high-burden settings (Gao et al., 2024). Incorporating environment-mediated TB transmission is therefore essential for a realistic depiction of TB dynamics. Environmental reservoirs can act as persistent sources of infection, undermining interventions that target only human populations. Explicitly modeling environmental TB contamination provides a more comprehensive framework to assess the combined impact of medical interventions and environmental control measures, such as hygiene and sanitation, on disease dynamics.

Despite the extensive body of mathematical models developed to study HIV–TB co-infection, several important gaps remain. Most existing models either rely on classical integer-order formulations that neglect memory effects inherent in chronic infections, or they focus exclusively on human-to-human transmission pathways while overlooking the role of environmentally mediated tuberculosis persistence. Furthermore, few studies integrate real epidemiological data to calibrate fractional-order co-infection models, and even fewer investigate the combined impact of medical and environmental interventions within an optimal control framework. Unlike existing HIV–TB models, this study simultaneously incorporates environmental TB reservoirs, fractional memory effects through the Caputo derivative, data-driven parameter estimation using WHO-reported HIV–TB co-infection data from Tanzania, and the optimal deployment of medical and environmental control strategies within a unified modeling framework. This thorough approach yields a more accurate representation of HIV–TB transmission dynamics and offers actionable insights for the design of integrated, data-driven, and sustainable disease control policies in high-burden settings.

The paper is structured as follows: Section 2 introduces the model and its assumptions. Section 3 examines the model's qualitative properties, including Ulam–Hyers stability, the PECE–ABM method, parameter estimation, and sensitivity analysis. Section 4 focuses on the HIV–TB co-infection model with control strategies, covering the effective reproduction number, optimal control formulation, and necessary conditions for optimality. Section 5 presents and discusses numerical simulations and control outcomes. Section 6 concludes with the main findings and implications for policy.

2. Mathematical model formulation

This section presents a fractional-order HIV–TB co-infection model formulated using the Caputo derivative to capture memory-dependent disease dynamics (Devi et al., 2025; Gemeda et al., 2025). Fractional calculus is particularly appropriate for chronic infections such as HIV and TB, where past exposure, delayed immune responses, treatment adherence, and environmental persistence influence current transmission patterns. To focus on the essential mechanisms governing HIV–TB co-infection, several modeling assumptions are adopted. It is assumed that individuals are recruited into the susceptible population at a constant rate Ω. The population is assumed to be homogeneous. It is assumed that susceptible individuals cannot simultaneously acquire both HIV and TB infections; thus, they cannot move directly to the co-infected class (Aggarwal and Raj, 2021). The model assumes no vertical (mother-to-child) HIV transmission (Ayele et al., 2024a; Devi et al., 2025). Tuberculosis transmission is assumed to occur via both direct contact with infectious individuals and exposure to environmental contamination (Gao et al., 2024). Individuals co-infected with HIV and active TB are assumed to be severely immunocompromised. Owing to their clinical condition, sexual activity within this class is considered negligible, and hence sexual transmission of HIV from this compartment is excluded (Ayele et al., 2024a). All individuals receiving antiretroviral therapy (ART) are assumed to be aware of their HIV status, to be under continuous clinical supervision, and to engage in behaviors that reduce onward transmission (Ayele et al., 2024a). In line with World Health Organization recommendations, TB screening is assumed to occur at HIV diagnosis and throughout the follow-up period, with immediate administration of TB treatment among co-infected

individuals (Ayele et al., 2024a; Mallela et al., 2016). Consequently, the model assumes that TB treatment precedes the initiation of HIV treatment in co-infected individuals. The standard duration of TB therapy is taken to be six to nine months (World Health Organization (WHO), 2023). Furthermore, Individuals undergoing treatment for HIV or TB are assumed to contribute negligibly to onward transmission. While a small residual transmission risk may persist during early treatment or in cases of imperfect adherence, clinical evidence indicates that effective therapy substantially reduces infectiousness by lowering viral and bacillary loads. Given the population-level focus of the model, transmission from treated individuals is therefore neglected. Individuals who recover from TB while remaining on ART are considered non-infectious due to sustained viral suppression. Finally, co-infected individuals who continue ART following TB recovery are assumed to adopt behaviors that reduce their risk of TB reinfection.

Based on these assumptions, the total human population $N(t)$ is stratified into nine mutually exclusive compartments: Susceptible (S), Latent TB (L), Active TB (A), Recovered from TB (R), HIV-infected (I), on ART (T_2), HIV-Latent TB co-infected (C_1), HIV-Active TB co-infected (C_2), and co-infected on TB treatment (T_1). A tenth compartment (B) models environmental TB bacilli concentration. Thus:

$$N(t) = S(t) + L(t) + A(t) + R(t) + I(t) + T_2(t) + C_1(t) + C_2(t) + T_1(t). \quad (1)$$

The force of infection for TB, χ_1, incorporates direct and environmental pathways:

$$\chi_1 = \left[\frac{\beta_T}{N}(A + q_1 C_2) + \beta_1 B\right], \quad (2)$$

where β_T is the direct TB transmission rate, β_1 is the environmental infection rate, and $q_1 > 1$ amplifies the infectiousness of C_2 individuals. The force of infection for HIV, χ_2, accounts for contact with infectious compartments:

$$\chi_2 = \frac{\beta_H}{N}(I + q_2 C_1), \quad (3)$$

where β_H is the HIV transmission rate and $q_2 > 1$ represents enhanced infectivity of C_1 individuals.

Susceptible individuals may acquire TB or HIV at rates χ_1 and χ_2, respectively. Those in the latent TB class (L) may progress to active TB at rate θ_1, or acquire HIV at rate χ_2. Also those in Latent class can start TB treatment at a rate τ_0 and move to recovery group. Individuals with active TB (A) may also contract HIV at rate χ_2, start TB treatment at rate τ, or die due to TB-related complications at rate d_1. Recovered individuals (R) remain susceptible to HIV infection at rate χ_2 and may be partially re-infected with TB at rate $\phi\chi_1$, where $\phi \in [0, 1]$ captures the degree of immunity from previous TB infection. HIV-infected individuals (I) may acquire TB at an increased rate $\delta\chi_1$ due to immunosuppression ($\delta > 1$), initiate ART at rate η, or die from HIV-related causes at rate d_2. Individuals in the C_1 class may progress to active TB co-infection (C_2) at rate θ_2, die at rate d_2, or initiate TB treatment at rate τ_1, consistent with guidelines prioritizing TB treatment before ART. Those in the C_2 class may start TB treatment at rate τ_2, transitioning to the T_1 class, or die from disease-related causes at rate d_3. Individuals in T_1 may subsequently initiate ART and move to T_2 at rate η or experience death due to disease at rate d_3. The environmental bacterial load B increases through shedding from A and C_2 (rates k_1, k_2) and decays naturally at rate m. Every human compartment experiences natural mortality at rate μ. The results of the above are summarized in Fig. 1

2.1. The Caputo fractional derivative model

The fractional-order formulation adopted in this study is biologically motivated by the strong memory and hereditary effects inherent in HIV–TB co-infection dynamics. HIV progression is characterized by cumulative immune system degradation, delayed virological response to antiretroviral therapy, and long-term treatment history, while tuberculosis exhibits prolonged latency, partial immunity, and reactivation after extended periods (Adeyemo et al., 2023; Ayele et al., 2024a). Moreover, the persistence of Mycobacterium tuberculosis in contaminated environments introduces additional temporal dependence, as current infection risk depends not only on present conditions but also on past pathogen shedding and environmental contamination levels (Gao et al., 2024). The Caputo fractional derivative is therefore employed to represent these effects, as it allows the present rate of change to depend on the entire history of the system while preserving biologically meaningful initial conditions (Lusekelo et al., 2023). Mathematically, this implies that each state variable evolves according to a convolution-type integral over its past values, which is formalized through the Caputo fractional derivative defined below. Consequently, the fractional-order derivative provides a realistic representation of delayed immune responses, treatment adherence history, and environmental persistence that cannot be adequately captured by classical integer-order models.

To ensure dimensional consistency in the fractional-order HIV–TB co-infection model, we adopt a fractional time-scaling approach commonly used with Caputo derivatives. Since the Caputo derivative of order $p \in (0, 1]$ has dimension $[\text{time}]^{-p}$, classical rate parameters must be rescaled to preserve dimensional homogeneity of the governing equations. Accordingly, all time-dependent parameters are raised to the fractional order p, restoring mathematical coherence of the model. This scaling should not be interpreted as a literal biological modification of epidemiological rates, but rather as a mathematical device that allows integer-order parameters to be consistently embedded within a fractional-order framework. Biologically, the fractional order p reflects memory effects associated with chronic infection, treatment history, and environmental persistence, and this approach is well established in fractional epidemiological modeling (Angstmann et al., 2016; Pinto and Carvalho, 2017; Ruoja et al., 2025).

$$\chi_1^C = \left[\frac{\beta_T^p}{N}(A + q_1 C_2) + \beta_1^p B\right] \quad \text{and} \quad \chi_2^C = \frac{\beta_H^p}{N}(I + q_2 C_1). \quad (4)$$

Considering the assumptions, the model flow diagram (Fig. 1), and the parameter definitions in Table 1, the HIV–TB co-infection dynamics are described by the following system of nonlinear differential equations under the Caputo fractional derivative:

$$\begin{cases}
{}_0^C D_t^p S(t) = \Omega^p - \left(\chi_1^C + \chi_2^C + \mu^p\right) S \\
{}_0^C D_t^p L(t) = \chi_1^C S + \phi\chi_1^C R - \left(\mu^p + \theta_1^p + \tau_0^p + \chi_2^C\right) L \\
{}_0^C D_t^p A(t) = \theta_1^p L - \left(\mu^p + d_1^p + \tau^p + \chi_2^C\right) A \\
{}_0^C D_t^p R(t) = \tau^p A + \tau_0^p L - \left(\mu^p + \phi\chi_1^C + \chi_2^C\right) R \\
{}_0^C D_t^p B(t) = k_1^p A + k_2^p C_2 - m^p B \\
{}_0^C D_t^p I(t) = \chi_2^C S + \chi_2^C R - \left(\mu^p + d_2^p + \delta\chi_1^C + \eta^p\right) I \\
{}_0^C D_t^p T_2(t) = (I + T_1)\eta^p - (\mu^p + d_2^p) T_2 \\
{}_0^C D_t^p C_1(t) = \chi_2^C L - \left(\mu^p + \theta_2^p + d_2^p + \tau_1^p\right) C_1 \\
{}_0^C D_t^p C_2(t) = \theta_2^p C_1 + \delta\chi_1^C I + \chi_2^C A - \left(\mu^p + d_3^p + \tau_2^p\right) C_2 \\
{}_0^C D_t^p T_1(t) = \tau_1^p C_1 + \tau_2^p C_2 - \left(\mu^p + \eta^p + d_3^p\right) T_1
\end{cases} \quad (5)$$

The model is subject to initial conditions

$$S(0) > 0, L(0) \geq 0, A(0) \geq 0, R(0) \geq 0, B(0) \geq 0, I(0) \geq 0, T_2(0) \geq 0,$$
$$C_1(0) \geq 0, C_2(0) \geq 0, T_1(0) \geq 0.$$

3. Analysis of HIV-TB co-infection model

Here, we investigate the qualitative behavior of the proposed fractional-order HIV–TB co-infection model, including well-posedness, computation of the basic reproduction number, local stability of the disease-free equilibrium, and Ulam–Hyers stability, with full technical proofs provided in the appendices.

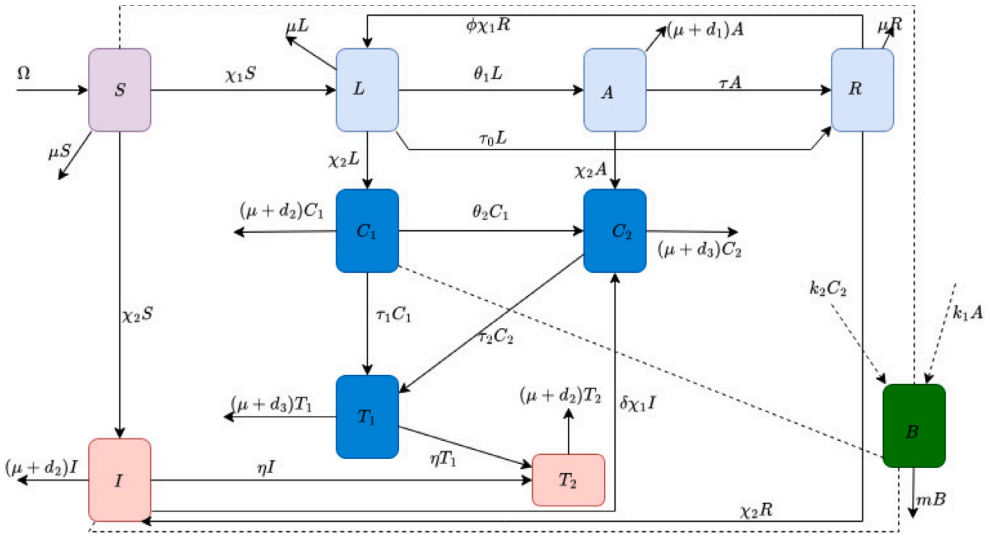

Fig. 1. Schematic representation of HIV–TB co-infection dynamics including environmental TB transmission.

Table 1
Parameter symbols, and their respective meaning.

Parameters	Biological meaning
Ω	Recruitment rate
β_H	HIV transmission rate
β_T	TB transmission coefficient
μ	Natural death rate
d_1	TB-related mortality rate
d_2	HIV-related mortality rate
d_3	Mortality rate due to TB–HIV co-infection
β_1	Environmental TB transmission coefficient
η	HIV treatment rate
q_1	Transmission amplification factor for TB in co-infected individuals (C_2).
q_2	Transmission amplification factor for TB in co-infected individuals (C_1).
δ	TB progression multiplier for HIV-positive individuals
ϕ	Re-infection risk modifier
θ_1	Rate at which latent TB progresses to active TB in HIV-negative individuals
θ_2	Rate at which latent TB progresses to active TB in HIV-positive individuals
τ	Per-capita treatment rate for individuals with active TB
τ_0	Treatment rate for individuals with latent TB
τ_1	Treatment rate for individuals with latent TB who are co-infected with HIV
τ_2	Treatment rate for Active TB (co-infected)
k_1	Bacterial shedding rate by active TB individuals (A)
k_2	Bacterial shedding rate by co-infected individuals (C_2)
m	Clearance rate of bacteria in the environment

3.1. Well-posedness

The well-posedness of the fractional-order system (5) is established by proving the existence, uniqueness, positivity, and boundedness of its solutions.

Theorem 1 (*Existence, Uniqueness, and Positivity*)**.** *For any non-negative initial conditions, system (5) possesses a unique solution which remains non-negative for all $t \geq 0$.*

Proof. Existence and uniqueness follow from standard results for Caputo fractional differential equations with locally Lipschitz right-hand sides (Huo et al., 2015). Positivity is verified by evaluating the Caputo derivative of each state variable on the boundary of the non-negative orthant. For example, when $S = 0$, we have ${}_0^C D_t^p S = \Omega^p > 0$, ensuring trajectories remain non-negative. A similar argument applies to all compartments. The full proof is given in Appendix A. □

Theorem 2 (*Boundedness and Positive Invariance*)**.** *All solutions of system (5) initiating in the biologically feasible region*

$$D = \left\{ \begin{matrix} (S, L, A, R, B, I, T_2, C_1, C_2, T_1) \in \mathbb{R}_+^{10} : \\ N \leq \dfrac{\Omega^p}{\mu^p}, \qquad B \leq \dfrac{(k_1^p + k_2^p)\Omega^p}{m^p \mu^p} \end{matrix} \right\}. \tag{6}$$

remain in D for all $t > 0$.

Proof. By summing the human population equations, we obtain a linear fractional differential equation for $N(t)$, whose solution is bounded above by Ω^p/μ^p. A similar comparison argument applies to the environmental bacterial load $B(t)$. The detailed Laplace transform-based derivation is provided in Appendix A.

These results confirm that the model is mathematically well-posed and epidemiologically meaningful. □

3.2. Disease-free equilibrium and basic reproduction number

The HIV–TB co-infection-free equilibrium (DFE) of system (5) is obtained by setting all infected compartments to zero, yielding

$$E^0 = \left(S^0, L^0, A^0, R^0, B^0, I^0, T_2^0, C_1^0, C_2^0, T_1^0\right) = \left(\frac{\Omega^p}{\mu^p}, 0, 0, 0, 0, 0, 0, 0, 0, 0\right). \tag{7}$$

To investigate the risk of disease transmission, we determine the basic reproduction number $\mathcal{R}_0$ using the next-generation matrix method as formulated in Naik et al. (2020a) and applied in Bolaji et al. (2024). The basic reproduction number measures the mean number of secondary infections caused by a single infectious individual in a fully susceptible population during their infectious period (Naik et al., 2020a; Bolaji et al., 2024). Since the diseases are independent at the DFE, the overall basic reproduction $\mathcal{R}_0$ is given by

$$\mathcal{R}_0 = \max\left\{\mathcal{R}_0^{TB}, \mathcal{R}_0^{HIV}\right\} \tag{8}$$

where,

$$\mathcal{R}_0^{TB} = \frac{\theta_1^p(\Omega^p \beta_1^p k_1^p + \beta_T^p m^p \mu^p)}{\mu^p(\mu^p + \theta_1^p + \tau_0^p) m^p (d_1^p + \mu^p + \tau^p)}. \tag{9}$$

and

$$\mathcal{R}_0^{HIV} = \frac{\beta_H^p}{\mu^p + d_2^p + \eta^p}. \tag{10}$$

The quantity $\mathcal{R}_0^{TB}$ captures both direct TB transmission and environment-mediated transmission, highlighting the role of bacterial persistence in sustaining TB spread. The HIV reproduction number $\mathcal{R}_0^{HIV}$ reflects the balance between HIV transmission and treatment induced removal. The full derivation, including Jacobian matrices, is presented in Appendix B.

3.3. Local stability analysis of the DFE

We analyze the local asymptotic stability of the disease-free equilibrium (DFE) E^0, which corresponds to a state free of both HIV and TB. Small perturbations near E^0 are examined using an eigenvalue-based method adapted from Edward (Edward, 2024). The stability condition is established by the following theorem.

Theorem 3. *The disease-free equilibrium E^0 of system (5) is locally asymptotically stable when $\mathcal{R}_0 < 1$, and unstable when $\mathcal{R}_0 > 1$.*

Proof. The result follows from analyzing the eigenvalues of the Jacobian matrix evaluated at E^0 and applying the fractional-order stability criterion, which requires that all eigenvalues satisfy

$$|\arg(\lambda_i)| \rangle \frac{\pi p}{2}.$$

Epidemiologically, this result implies that both HIV and TB can be eliminated if their respective reproduction numbers are reduced below unity. The detailed proof of eigenvalue-based argument of Theorem 3 is provided in Appendix C. □

3.4. Ulam–Hyers stability analysis

A model's practical utility depends on its robustness to perturbations, such as those from parameter uncertainty or numerical approximation. To establish this property, we analyze the Ulam–Hyers stability of our fractional-order system, which guarantees that approximate solutions remain close to true solutions under small disturbances.

Theorem 4. *The Caputo fractional-order HIV–TB co-infection model (5) exhibits Ulam–Hyers stability on the time interval $[0, T]$ if the following condition holds:*

$$\Gamma(p+1) > \kappa T^p,$$

where κ is the Lipschitz constant associated with the model vector field.

Proof. Ulam–Hyers stability guarantees that approximate solutions remain close to exact solutions, even when the governing equations are subject to small perturbations. This property is particularly important for models calibrated with real epidemiological data. Unlike classical Lyapunov stability, which examines the behavior of exact solutions under infinitesimal perturbations of initial conditions.

The complete proof is deferred to Appendix D. □

3.5. PECE–ABM algorithm for solving Caputo fractional order system

Numerical solutions for the Caputo fractional-order system (5) were generated using the PECE-ABM (Predict-Evaluate-Correct-Evaluate Adams–Bashforth–Moulton) algorithm, a multi-step method chosen for its efficacy in handling the memory integrals inherent in fractional derivatives (Naik et al., 2020b). The PECE-ABM method proceeds through an explicit predictor step (Adams–Bashforth) followed by an implicit corrector step (Adams–Moulton). For numerical implementation, we define a fixed step size h and discretize the time domain into grid points $t_k = kh$. Considering the initial value problem in Eq. (5), the predictor step uses weights

$$c_{l,k+1} = \frac{h^p}{p}\left[(k+1-l)^p - (k-l)^p\right],$$

to generate predicted values:

$$\tilde{y}_{n+1} = y_0 + \frac{1}{\Gamma(p)}\sum_{l=0}^{k} c_{l,k+1} G_l,$$

which are then evaluated to obtain $\tilde{G}_{k+1} = G(t_{k+1}, \tilde{y}_{k+1})$.

Subsequently, the corrector step refines the solution using weights

$$d_{l,k+1} = \frac{h^p}{p(p+1)}\left[(k+1-l)^{p+1} - (k-l)^{p+1}\right],$$

yielding:

$$y_{n+1} = y_0 + \frac{1}{\Gamma(p)}\left(\sum_{l=0}^{k} d_{l,k+1} G_l + h^p \tilde{G}_{k+1}\right).$$

The corrected solution is then re-evaluated as $G_{k+1} = G(t_{k+1}, y_{k+1})$. This iterative prediction–evaluation–correction–evaluation framework is applied to each compartment of the model, such as susceptible, infected, and treated populations, updating the force of infection, and total population size at each step. The scheme ensures stable and accurate numerical integration of the fractional-order dynamics, making it suitable for simulating controlled and uncontrolled scenarios in co-infection models over extended time horizons.

3.6. Parameter estimation

To calibrate system (5), parameters were estimated using WHO-reported HIV–TB co-infection data for Tanzania covering 2000 to 2023, expressed as cases per 100,000 population (World Health Organization, 2023a). The data are publicly available, aggregated, and anonymized, requiring no ethical approval. Model calibration was performed by fitting the HIV–active TB co-infected compartment $C_2(t)$, which directly corresponds to the reported data and captures the synergistic HIV–TB interaction driving transmission and environmental contamination, while all other compartments were indirectly constrained by the model structure. Initial conditions were derived from demographic and epidemiological data for the year 2000, with $C_2(0) = 309$; infected compartments were inferred from prevalence data, treated compartments were assumed initially small, and the environmental TB load was taken proportional to infectious TB cases, ensuring biological feasibility. Parameter estimation was performed by minimizing the discrepancy between the observed HIV–TB co-infection data and the model predicted co-infected population. Let $C_2^{\text{data}}(t_i)$ denote the reported HIV–TB co-infection data at time t_i, and $C_2^{\text{model}}(t_i \mid \theta)$ denote the corresponding model output for a parameter vector θ. The objective function was defined using the root mean square error (RMSE) as

$$\text{RMSE}(\theta) = \left[\frac{1}{n}\sum_{i=1}^{n}\left(C_2^{\text{data}}(t_i) - C_2^{\text{model}}(t_i \mid \theta)\right)^2\right]^{1/2}, \tag{11}$$

where $n = 24$ and θ denotes selected transmission, progression, and environmental parameters. The fractional system was solved using the PECE-ABM scheme outlined in Section 3.5, and optimization was performed via the Nelder–Mead simplex algorithm (Chinyoka et al., 2021) in MATLAB. Demographic parameters were obtained from national life expectancy data. For Tanzania, with an average life expectancy of approximately 66.8 years (World Health Organization, 2023b), yielding a natural mortality rate of $\mu = 1/66.8 \approx 0.0147\,\text{year}^{-1}$, with recruitment adjusted to maintain population balance.

The quality of the fit was assessed using the root mean square error (RMSE), which reached a minimum value of 8.06 at the fractional order $p = 0.982$ (Fig. 2). RMSE decreases as p approaches 0.982 and increases for lower values, indicating that $p = 0.982$ is the optimal fractional derivative order for the given data. Fig. 3(a) shows the model estimates

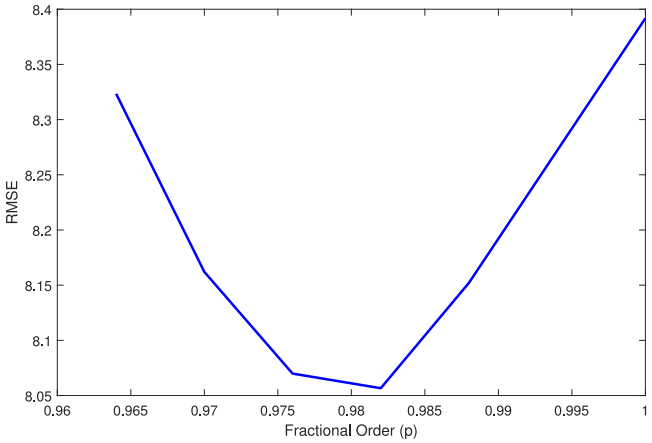

Fig. 2. Root Mean Square Error (RMSE) analysis across derivative orders.

corresponding to this optimal order. Fig. 3(b) compares integer order and fractional-order model predictions, revealing that the fractional-order model (RMSE = 8.06, $R^2 = 0.9915$) outperforms the integer-order model (RMSE = 8.39, $R^2 = 0.9907$), achieving an approximately 4% reduction in RMSE and a marginally improved goodness-of-fit. The resulting parameters are presented in Table 4.

3.6.1. Model validation

To examine the generalizability of the fractional-order HIV–TB co-infection model, an independent validation was performed using WHO-reported Kenya HIV–TB co-infection data from 2000–2023 (World Health Organization, 2023a). Kenya was selected due to its geographical proximity to Tanzania and comparable epidemiological and socioeconomic characteristics, while representing an independent population. All epidemiological parameters estimated from Tanzanian data were retained, assuming conservation of underlying biological and behavioral processes across East African settings. Only demographic parameters were adjusted to reflect Kenya specific characteristics: recruitment rate $\Omega = 7.8$ individuals per 100,000 per year and natural mortality rate $\mu = 0.0150$ per year, based on a life expectancy of 66.8 years (World Health Organization, 2023c). Initial conditions were calibrated to match Kenya's 2000 HIV–TB prevalence. The model ($p = 0.982$) was simulated through 2023 and compared with observed data (Fig. 4).

Model performance on the validation dataset was evaluated using RMSE, MAPE, and R^2, yielding RMSE = 13.17, MAPE = 21.18%, and $R^2 = 0.9601$, indicating good predictive accuracy. The model successfully reproduced key temporal features of Kenya's HIV–TB co-infection dynamics, including the peak during 2005–2007 and the subsequent decline following ART scale-up. Deviations observed during the peak period likely reflect differences in intervention coverage or behavioral factors not captured through demographic parameter adjustments, highlighting the robustness of the fractional-order framework.

3.7. Sensitivity analysis

To evaluate the relative influence of model parameters, a sensitivity analysis of the basic reproduction numbers $\mathcal{R}_0$ is performed. Such analysis identifies the parameters that most significantly affect disease transmission dynamics and quantifies how small changes in these parameters influence the model outcomes. The normalized forward sensitivity index (Chitnis et al., 2008) is used to calculate how a small percentage change in a parameter **k** affects the reproduction number. The sensitivity of $\mathcal{R}_0^{TB}$ or $\mathcal{R}_0^{HIV}$ to its parameters is evaluated using the index

$$Y_k = \frac{k}{\mathcal{R}_0^{TB}} \times \frac{\partial \mathcal{R}_0^{TB}}{\partial k}.$$

Table 2
Sensitivity indices of model parameters for the basic reproduction numbers $\mathcal{R}_0^{TB}$ and $\mathcal{R}_0^{HIV}$.

Parameter (k)	Index (Y_k)	Parameter (k)	Index (Y_k)	Parameter (k)	Index (Y_k)
β_H	1	d_1	0.3640	m	−0.7913
Ω	0.7913	d_2	0.3571	τ_0	−0.6828
β_1	0.7913	β_T	0.2087	τ	−0.5828
k_1	0.7913	μ	0.0714	η	−0.5714
θ_1	0.400	ϕ	0		

The resulting indices, computed at $p = 0.982$, are presented in Table 2. The computed sensitivity indices highlight a crucial insight: increasing the negatively sensitive parameters (τ, η, m) effectively suppresses disease dynamics, thereby offsetting transmission, while positively sensitive parameters such as k_1, β_T, β_H, and β_1 promote disease spread. Quantitatively, $\mathcal{R}_0^{TB}$ and $\mathcal{R}_0^{HIV}$ are reduced by 7.9% and 5.7%, respectively, for a 10% increase in m and η. This mechanistic understanding directly informs and validates the choice of multi-faceted environmental and medical controls presented in Section 4.

To examine the robustness of these sensitivity results under parameter uncertainty, confidence intervals for the normalized sensitivity indices were computed using a Monte Carlo uncertainty propagation approach. Model parameters were sampled from truncated normal distributions consistent with their estimated means and 95% confidence intervals reported in Table 4, and sensitivity indices were recalculated for each realization using the analytical expressions of the fractional-order model. Empirical 95% confidence intervals were obtained from the percentile distributions of the resulting sensitivity indices, as summarized in Table 3. The results confirm that the sign and relative ranking of the most influential parameters remain stable across uncertainty ranges, with key transmission and treatment parameters exhibiting confidence intervals that do not include zero, thereby reinforcing the robustness of the sensitivity conclusions.

4. System with controls

To evaluate intervention strategies, the model (5) is extended to include time-dependent controls: $u_1(t)$, corresponding to TB case-finding and prompt treatment; $u_2(t)$, reflecting ART administration and adherence counseling to suppress viral load and restore immunity; and $u_3(t)$, denoting environmental hygiene and sanitation efforts aimed at reducing Mycobacterium tuberculosis concentration in the environment. The case-finding mitigates latent TB activation, ART lowers infectiousness, and environmental hygiene and sanitation diminishes environmentally mediated transmission. Consequently, the transmission dynamics under Caputo fractional derivatives are governed by the following system of nonlinear differential equations, derived from model system Eq. (5):

$$\begin{cases}
{}_0^C D_t^p S(t) = \Omega^p - \left(\chi_1^C + \chi_2^C + \mu^p\right) S \\
{}_0^C D_t^p L(t) = \chi_1^C S + \phi\chi_1^C R - \left(\mu^p + \theta_1^p + \tau_0^p + u_1 + \chi_2^C\right) L \\
{}_0^C D_t^p A(t) = \theta_1^p L - \left(\mu^p + d_1^p + \tau^p + u_1 + \chi_2^C\right) A \\
{}_0^C D_t^p R(t) = (\tau^p + u_1)A + (\tau_0^p + u_1)L - \left(\mu^p + \phi\chi_1^C + \chi_2^C\right) R \\
{}_0^C D_t^p B(t) = k_1^p A + k_2^p C_2 - (m^p + u_3)B \\
{}_0^C D_t^p I(t) = \chi_2^C S + \chi_2^C R - \left(\mu^p + d_2^p + \delta\chi_1^C + \eta^p + u_2\right) I \\
{}_0^C D_t^p T_2(t) = (I + T_1)(\eta^p + u_2) - (\mu^p + d_2^p)T_2 \\
{}_0^C D_t^p C_1(t) = \chi_2^C L - \left(\mu^p + \theta_2^p + d_2^p + \tau_1^p + u_1\right) C_1 \\
{}_0^C D_t^p C_2(t) = \theta_2^p C_1 + \delta\chi_1^C I + \chi_2^C A - \left(\mu^p + d_3^p + \tau_2^p + u_1\right) C_2 \\
{}_0^C D_t^p T_1(t) = (\tau_1^p + u_1)C_1 + (\tau_2^p + u_1)C_2 - \left(\mu^p + \eta^p + u_2 + d_3^p\right) T_1
\end{cases} \tag{12}$$

with,

$$\chi_1^C = \left[\frac{\beta_T^p}{N}(A + q_1 C_2) + \beta_1^p B\right] \quad \text{and} \quad \chi_2^C = \frac{\beta_H^p}{N}(I + q_2 C_1). \tag{13}$$

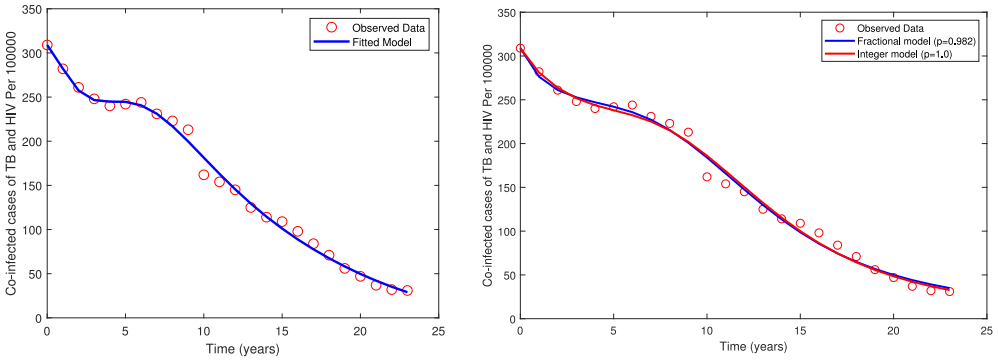

Fig. 3. HIV–TB co-infection prevalence in Tanzania (2000–2023) and model fits. (a) Fractional-order model ($p = 0.982$) estimation compared to reported data. (b) Comparative performance of fractional-order ($p = 0.982$) versus integer-order ($p = 1$) models.

Table 3
Mean normalized sensitivity indices and corresponding 95% confidence intervals (CI) for statistically significant parameters influencing $\mathcal{R}_0^{TB}$ and $\mathcal{R}_0^{HIV}$.

$\mathcal{R}_0^{TB}$			$\mathcal{R}_0^{HIV}$		
Parameter	Mean (Υ_k)	95% CI	Parameter	Mean (Υ_k)	95% CI
Ω	0.7824	[0.7661, 0.7981]	β_H	0.9820	[0.9820, 0.9820]
β_T	0.1996	[0.1839, 0.2159]	μ	−0.0433	[−0.0449, −0.0418]
μ	−0.9343	[−0.9503, −0.9174]	d_2	−0.3626	[−0.3791, −0.3460]
d_1	−0.4892	[−0.5070, −0.4709]	η	−0.5761	[−0.5928, −0.5592]
β_1	0.7824	[0.7661, 0.7981]			
θ_1	0.7583	[0.7468, 0.7695]			
τ	−0.4318	[−0.4494, −0.4144]			
τ_0	−0.6675	[−0.6802, −0.6543]			
k_1	0.7824	[0.7661, 0.7981]			
m	−0.7824	[−0.7981, −0.7661]			

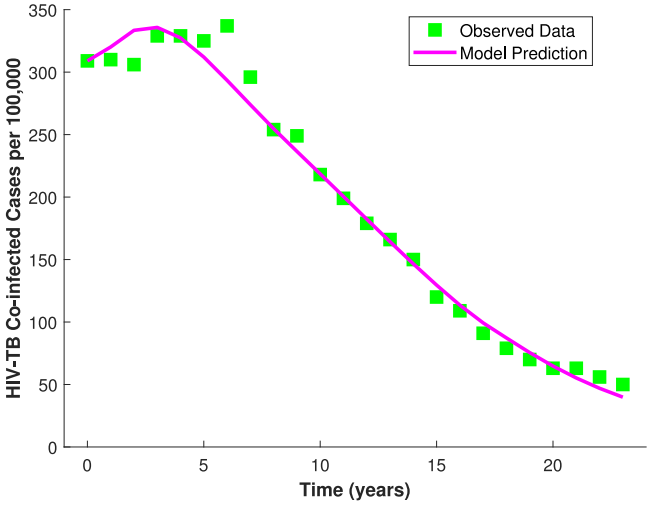

Fig. 4. Validation of the fractional-order HIV–TB co-infection model using Kenya data (2000–2023). Green squares indicate WHO-reported observations, and magenta curves show model predictions at $p = 0.982$.

Table 4
Parameters symbol, values, sources, estimates, confidence interval and units for HIV–TB co-infection model.

Parameter	Value	Source	Unit
Ω	15	Computed	persons year^{-1}
β_H	0.548	Fitted	year^{-1}
β_T	0.139	Fitted	year^{-1}
μ	0.0147	World Health Organization (2023b)	year^{-1}
d_1	0.1	Teklu et al. (2023)	year^{-1}
d_2	0.2	Zahli et al. (2024)	year^{-1}
d_3	0.33	Teklu et al. (2023)	year^{-1}
β_1	0.00292 (0-1)	Li and Wang (2023)	year^{-1}
η	0.16	Awoke and Kassa (2018)	year^{-1}
q_1	2	Fitted	dimensionless
q_2	3	Fitted	dimensionless
δ	4	Fitted	dimensionless
ϕ	0.001	Fitted	dimensionless
θ_1	0.03	Seidu et al. (2023)	year^{-1}
θ_2	0.2	Awoke and Kassa (2018)	year^{-1}
τ	0.16	Awoke and Kassa (2018)	year^{-1}
τ_0	0.153	Ayele et al. (2024a)	year^{-1}
τ_1	0.2	Awoke and Kassa (2018)	year^{-1}
τ_2	0.2	Ayele et al. (2024a)	year^{-1}
k_1	0.45	Li and Wang (2023)	Day^{-1}
k_2	0.676	Fitted	Day^{-1}
m	0.60	Li and Wang (2023)	Day^{-1}

4.1. Effective reproduction number $\mathcal{R}_e$

The influence of intervention strategies on the dynamics of HIV–TB co-infection is evaluated through the effective reproduction number, $\mathcal{R}_e$. This quantity measures the expected number of new infections arising from a single infectious individual in a partially controlled population (Stephano et al., 2024). Following the methodology outlined in Section 3.2 and employing the established next-generation matrix approach (Naik et al., 2020a; Bolaji et al., 2024), $\mathcal{R}_e$ for the system in Eq. (12) is determined as:

$$\mathcal{R}_e = \max\left\{\mathcal{R}_e^{HIV}, \mathcal{R}_e^{TB}\right\} \tag{14}$$

Since the two diseases are independent at the DFE, their effective reproduction numbers are computed separately. The effective reproduction

number for the TB subsystem is

$$\mathcal{R}_e^{TB} = \frac{\theta_1^p \left(\Omega^p \beta_1^p k_1^p + \beta_T^p m^p \mu^p + \beta_T^p \mu^p u_3\right)}{\mu^p(\mu^p + \theta_1^p + \tau_0^p + u_1)(m^p + u_3)(d_1^p + \mu^p + \tau^p + u_1)}. \tag{15}$$

The effective reproduction number for the HIV subsystem is

$$\mathcal{R}_e^{HIV} = \frac{\beta_H^p}{\mu^p + d_2^p + \eta^p + u_2}. \tag{16}$$

These expressions account for transmission from individuals with active TB, the contaminated environment, and direct HIV spread, all modulated by the applied controls. The results emphasize the theoretical impact of the interventions: increasing case-finding and treatment for TB (u_1), ART (u_2), and environmental hygiene and sanitation (u_3) directly reduces the transmission potential of the co-infection. The detailed derivation of the effective reproduction number presented in Appendix E.

4.2. Optimal control problem

To design optimal control strategies, we focus on reducing the key compartments that sustain HIV–TB co-infection: the contaminated environment (B), which serves as a transmission reservoir, and the infected classes (L, A, I C_1, and C_2), which are primary drivers of spread. Minimizing the sizes of L, A, I, C_1, C_2, and B thus addresses both direct transmission routes and critical behavioral determinants, forming an epidemiologically grounded and policy-relevant goal. Accordingly, based on system (12), we seek to identify an optimal control triple (u_1, u_2, u_3) that reduces infected populations, environmental contamination, and cost associated with control measures. Following the framework proposed by Ullah et al. (2025), Kheiri and Jafari (2018), the objective functional associated with Eq. (12) is defined as:

$$\begin{aligned} \mathcal{J}(u_1,u_2,u_3) &= \int_0^T \left[G_1 L + G_2 A + G_3 I + G_4 C_1 + G_5 C_2 + G_6 B + \frac{1}{2}\sum_{i=1}^{3} w_i u_i^2\right], dt \\ &= \int_0^T \ell(t,x,u)\, dt, \end{aligned} \tag{17}$$

where $\ell(t,x,u)$ represents the running cost. For a given co-state variable λ_n, the associated Hamiltonian is given by

$$\mathcal{H} = \ell(t,x,u) + \sum_{n=1}^{10} \lambda_n f_n(t,x,u) \tag{18}$$

The positive constants G_i ($i = 1,2,3,4,5,6$) quantify the relative importance of the state variables, while w_i ($i = 1,2,3$) represent the costs associated with implementing the control measures over the finite time horizon T. These constants prevent any one term from dominating the integral in the objective functional (Ullah et al., 2025; Kheiri and Jafari, 2018). Additionally, the objective function is expressed quadratically for ease of computation (Karim et al., 2023; Liu et al., 2024). The admissible control set for $i = 1,2,3$ is defined by

$$U = \{(u_1,u_2,u_3) \mid u_i \text{ is Lebesgue measurable and } 0 \le u_i \le 1,\ t \in [0,T]\}.$$

The optimal control $u^* = (u_1^*, u_2^*, u_3^*) \in U$ minimizes the objective functional:

$$J(u^*) = \min_{(u_1,u_2,u_3)\in U} J(u_1,u_2,u_3).$$

4.3. Characterization of optimal control problem

Under the well-posed structure of the state system and the uniform L^∞ bounds on admissible states and controls, classical results guarantee the existence of an optimal control (Ayele et al., 2024a; Sinan et al., 2021). To derive the necessary optimality conditions for the control (u^*), Pontryagin's Maximum Principle adapted for fractional-order systems governed by the Caputo derivative is employed (Lenhart and Workman, 2007; Pontryagin, 2018). This principle transforms system Eq. (12), together with the objective functional Eq. (17), into a pointwise minimization of the Hamiltonian ($\mathcal{H}$) with respect to the controls ($u_i(t)$) (Naik et al., 2020b; Okyere et al., 2020). For optimality to hold in the fractional setting, the Hamiltonian ($\mathcal{H}$) must satisfy the fractional state dynamics, the fractional adjoint system, and the associated stationarity conditions. As from (Lusekelo et al., 2023; Kheiri and Jafari, 2018), the corresponding fractional state dynamics, adjoint system and stationarity conditions are derived as: The state dynamics given by ${}_0^C D_t^p f_n = \frac{\partial \mathcal{H}}{\partial \lambda_n}$, and adjoint system given by ${}_0^C D_t^p \lambda_n = -\frac{\partial \mathcal{H}}{\partial x_n}$. Therefore, the system of adjoint variable takes the form:

$$\begin{cases}
{}_0^C D_t^p \lambda_S(t) &= \chi_1^C \left(\lambda_S - \lambda_L\right) + \chi_2^C \left(\lambda_S - \lambda_I\right) + \mu^p \lambda_S \\
{}_0^C D_t^p \lambda_L(t) &= -G_1 + \chi_2^C \left(\lambda_L - \lambda_{C_1}\right) + \theta_1^p \left(\lambda_L - \lambda_A\right) + \left(\tau_0^p + u_1\right)\left(\lambda_L - \lambda_R\right) + \mu^p \lambda_L \\
{}_0^C D_t^p \lambda_A(t) &= -G_2 + \phi \frac{\beta_T^p}{N} R \left(\lambda_R - \lambda_L\right) + \frac{\beta_T^p}{N} S \left(\lambda_S - \lambda_L\right) + \delta \frac{\beta_T^p}{N} I \left(\lambda_I - \lambda_{C_2}\right) \\
&\quad + \left(\tau^p + u_1(t)\right)\left(\lambda_A - \lambda_R\right) - k_1^p \lambda_B + \left(\mu^p + d_1^p\right)\lambda_A - \chi_2^C \lambda_A \\
{}_0^C D_t^p \lambda_R(t) &= \phi \chi_1^C \left(\lambda_R - \lambda_L\right) + \chi_2^C \left(\lambda_R - \lambda_I\right) + \mu^p \lambda_R \\
{}_0^C D_t^p \lambda_B(t) &= -G_6 + \beta_1^p \delta \left(\lambda_S - \lambda_L\right) + \phi \beta_1^p R \left(\lambda_R - \lambda_L\right) \\
&\quad + \beta_1^p \delta I \left(\lambda_I - \lambda_{C_2}\right) + \left(m^p + u_3(t)\right)\lambda_B \\
{}_0^C D_t^p \lambda_I(t) &= -G_3 + \frac{\beta_H^p}{N} S \left(\lambda_S - \lambda_I\right) + \frac{\beta_H^p}{N} R \left(\lambda_R - \lambda_I\right) + \frac{\beta_H^p}{N} L \left(\lambda_L - \lambda_{C_1}\right) \\
&\quad + \frac{\beta_H^p}{N} A \left(\lambda_A - \lambda_{C_2}\right) \\
&\quad + \left(\eta^p + u_2(t)\right)\left(\lambda_I - \lambda_{T_2}\right) + \delta \chi_1^C \left(\lambda_I - \lambda_{C_2}\right) + \left(\mu^p + d_2^p\right)\lambda_I \\
{}_0^C D_t^p \lambda_{T_2}(t) &= \left(\mu^p + d_2^p\right) \lambda_{T_2} \\
{}_0^C D_t^p \lambda_{C_1}(t) &= -G_4 + q_2 \frac{\beta_H^p}{N} S \left(\lambda_S - \lambda_I\right) + q_2 \frac{\beta_H^p}{N} R \left(\lambda_R - \lambda_I\right) \\
&\quad + q_2 \frac{\beta_H^p}{N} A \left(\lambda_A - \lambda_{C_2}\right) + q_2 \frac{\beta_H^p}{N} L \left(\lambda_L - \lambda_{C_1}\right) \\
&\quad + \left(\tau_1^p + u_1(t)\right)\left(\lambda_{C_1} - \lambda_{T_1}\right) + \theta_2^p \left(\lambda_{C_1} - \lambda_{C_2}\right) + \left(\mu^p + d_2^p\right)\lambda_{C_1} \\
{}_0^C D_t^p \lambda_{C_2}(t) &= -G_5 + q_1 \frac{\beta_T^p}{N} S \left(\lambda_S - \lambda_L\right) + q_1 \phi \frac{\beta_T^p}{N} R \left(\lambda_R - \lambda_L\right) + q_1 \delta \frac{\beta_T^p}{N} I \left(\lambda_I - \lambda_{C_2}\right) \\
&\quad + \left(\tau_2^p + u_1(t)\right)\left(\lambda_{C_2} - \lambda_{T_1}\right) - k_2^p \lambda_B + \left(\mu^p + d_3^p\right)\lambda_{C_2} \\
{}_0^C D_t^p \lambda_{T_1}(t) &= \left(\eta^p + u_2(t)\right)\left(\lambda_{T_1} - \lambda_{T_2}\right) + \left(\mu^p + d_3^p\right)\lambda_{T_1}
\end{cases} \tag{19}$$

Each adjoint variable $\lambda_n(t)$ satisfies the terminal condition $\lambda_n(T) = 0$ for $n = S, L, A, \ldots, T_1(1, 2,3, \cdots,10)$. The stationary conditions are derived by solving $0 = \frac{\partial \mathcal{H}}{\partial u_i}$, $\quad i = 1,2,3$. Hence,

$$u_1^* = \frac{L^*(\lambda_L - \lambda_R) + A^*(\lambda_A - \lambda_R) + C_1^*(\lambda_{C_1} - \lambda_{T_1}) + C_2^*(\lambda_{C_2} - \lambda_{T_1})}{w_1}$$

$$u_2^* = \frac{I^*(\lambda_I - \lambda_{T_2}) + T_1^*(\lambda_{T_1} - \lambda_{T_2})}{w_2}$$

$$u_3^* = \frac{B^* \lambda_B}{w_3}.$$

The optimal controls u_i^* ($i = 1,2,3$) are restricted to the interval $[0,1]$ and enforced through the projection formula

$$u_i^* = \max\{0, \min(u_i, 1)\}.$$

5. Numerical results and discussion

The optimal control strategies u^* for minimizing HIV–TB co-infection transmission at minimal cost are computed by numerically solving the Caputo-type fractional-order system in Eq. (12) using the PECE–ABM scheme outlined in Section 3.5. The forward–backward sweep technique (Lenhart and Workman, 2007; McAsey et al., 2012) iteratively integrates the state system forward, the adjoint system backward, and updates the control variables until convergence. This framework effectively captures the memory effects inherent in fractional-order dynamics while ensuring numerical accuracy and stability.

In optimal control problems, the cost weights w_i in the objective functional (17) represent the relative economic burden associated with implementing each intervention. These weights are introduced to balance epidemiological benefits against implementation costs and are commonly modeled using quadratic terms to penalize excessive control effort and to ensure convexity of the objective functional, thereby avoiding unrealistic or singular control solutions (Liu et al., 2024; Lenhart and Workman, 2007). In this study, the weights w_1, w_2, w_3 were selected to reflect approximate annualized per-capita costs reported in health economic studies from Tanzania and comparable sub-Saharan African settings. Here, w_1, w_2, and w_3 correspond respectively to TB treatment interventions, HIV treatment, and environmental control as defined in Section 4. Specifically, published estimates indicate that the cost of diagnosing and treating a single TB case in Tanzania ranges between USD 150-155 per person per year (Kilale et al., 2022). Accordingly, the weight associated with the TB treatment control was set to $w_1 = 150$ USD/person/year, representing a conservative estimate within this range.

Similarly, the annual cost of HIV treatment via antiretroviral therapy (ART) in Tanzania has been reported to range from USD 90 to 265 per person per year (McBain et al., 2023). Based on this range, the weight corresponding to HIV treatment was set to $w_2 = 150$ USD/person/year, reflecting a mid-range estimate. Environmental interventions such as disinfection, improved ventilation, and sanitation are typically implemented at the community level and involve shared, non-recurrent costs rather than individualized clinical expenditures. To capture this distinction, the cost weight associated with environmental control was assumed to be substantially lower and set to approximately 36% of the TB treatment cost, yielding $w_3 = 54$ USD/person/year. This assumption reflects the comparatively lower per-capita economic burden of environmental interventions while preserving the relative cost structure among controls. Overall, these weights are not intended to represent precise economic valuations but rather to provide a realistic and policy-relevant scaling of intervention costs, enabling meaningful comparison of optimal control strategies.

The weighting parameters G_i in the objective functional are chosen to reflect the severity of each compartment. The weight G_1 is associated with compartment L is assigned a weight in the interval $[0, 0.5]$ because less infectious compared to individuals in other infected compartments. The weight G_2 and G_3, associated with compartments A and I, are selected from the interval $[0.5, 1.5]$ due to their relatively lower immediate health and economic impacts compared to co-infected compartments. The co-infected compartments C_1 and C_2 are assigned a higher weights $G_4 \in [1, 5]$ and $G_5 \in [5, 10]$, respectively, to reflect its increased severity. The environmental bacterial load B, which contributes to prolonged infection and disease recurrence, is penalized with $G_6 \in [0, 0.5]$. Initial conditions are set accordingly, and model parameters are determined based on empirical data and existing literature, as presented in Table 4. Some parameters are adopted purely for numerical illustration due to data scarcity, which remains a notable limitation in modeling HIV–TB co-infection dynamics. The lack of high resolution, longitudinal data on environmental TB contamination, co-infection incidence, and behavioral factors introduces uncertainty in parameter estimates, as reflected in the wide confidence intervals for several fitted parameters (Table 4). This uncertainty propagates through the model, affecting the precision of long-term predictions and the estimated timing of intervention effects. For instance, variations in the environmental transmission rate (β_1) or bacterial clearance rate (m) could alter the predicted magnitude and timing of the impact of environmental interventions. From a policy perspective, this implies that model outputs should be interpreted primarily in a comparative and strategic sense, informing the relative effectiveness and prioritization of integrated interventions rather than precise quantitative forecasts. As more detailed data become available, model predictions and policy recommendations can be refined accordingly.

MATLAB is applied to execute the simulations and confirm the analytical findings. State trajectories and control profiles are analyzed for both controlled and uncontrolled cases. Considering both the endemicity of HIV–TB co-infection and the limited impact of single interventions (Ayele et al., 2024a, 2021, 2024b), we examine the effectiveness of multiple control strategies implemented concurrently over a five year period.

5.1. Optimal control strategies

To evaluate the synergistic effects of interventions, we defined and simulated multiple combined strategies. Starting from the three individual controls; TB case finding and treatment (u_1), HIV treatment (u_2), and environmental hygiene and sanitation (u_3), we constructed all non-trivial combinations comprising at least two controls. This resulted in four distinct strategies: three pairwise combinations (Strategies A-C), and one comprehensive combination employing all three controls simultaneously (Strategy D).

5.1.1. TB and HIV treatment (Strategy A)

This strategy emphasizes the simultaneous treatment of TB and HIV, a critical approach for managing co-infected individuals and reducing associated morbidity and mortality. As shown in Fig. 5(a) and 5(b), implementing combined HIV and TB treatment leads to a sharp decline in both latent and active co-infected cases relative to the no control scenario. Fig. 5(c) further indicates that both treatment controls, $u_1(t)$ and $u_2(t)$, are sustained at maximum intensity for approximately 3.58 and 3.25 years, respectively, after which they progressively decrease and approach zero by the end of the five-year time horizon. This extended period of full intervention reinforces the importance of sustained funding, adherence support, and integrated care models in real-world co-infection control programs. From a public health perspective, this control profile supports early scale-up of integrated HIV–TB co-infection services, including routine TB screening among people living with HIV, rapid initiation of ART, and sustained treatment delivery for at least three years to achieve meaningful reductions in co-infection burden.

5.1.2. TB treatment and environmental disinfection and improved sanitation(Strategy B)

This integrated strategy combines TB case finding and treatment with environmental hygiene and sanitation, thereby addressing both human-to-human and environmental transmission pathways. As shown in Fig. 6(a) and 6(b), implementation of these interventions leads to a significant decline in co-infected populations (both latent and active) relative to the no intervention scenario. Fig. 6(c) illustrates the corresponding control profiles: TB treatment efforts ($u_1(t)$) are maintained at maximum intensity for approximately 4.56 years before declining to zero, whereas environmental hygiene and sanitation ($u_3(t)$) initiates later, reaching full intensity after 3.1 years, sustained for five months, and then decreasing. This phased approach suggests an optimal resource allocation where clinical interventions are prioritized initially, followed by targeted environmental measures to consolidate gains and further reduce transmission risks in high-burden settings. In practical terms, this control profile supports strengthening TB case detection and treatment alongside sustained investments in environmental hygiene measures, including improved ventilation, sanitation, and infection prevention in high risk community and healthcare settings, to suppress ongoing tuberculosis transmission.

5.1.3. HIV treatment and environmental hygiene and sanitation (strategy C)

This strategy combines antiretroviral therapy (ART, $u_2(t)$) with environmental hygiene and sanitation for TB ($u_3(t)$), aiming to reduce TB susceptibility among immunocompromised individuals by addressing both host immunity and environmental exposure. As shown in Fig.

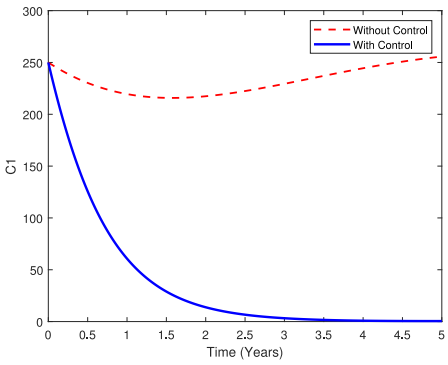

(a) Time evolution of HIV and latent TB co-infected individuals $C_1(t)$

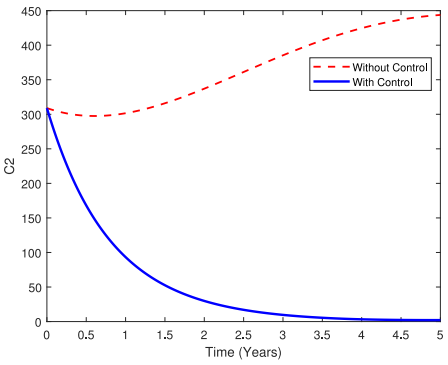

(b) Time evolution of HIV and active TB co-infected individuals $C_2(t)$

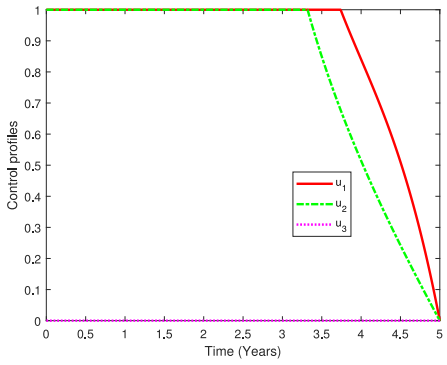

(c) Control profile

Fig. 5. Impact of combined TB and HIV treatment (Strategy A) at $p = 0.982$.

7(a) and 7(b), implementing these interventions results in a dramatic decrease in both latent and active TB co-infected populations relative to the no intervention baseline. The corresponding control profiles in Fig. 7(c) indicate that both ART and environmental hygiene and sanitation are maintained at maximum intensity for substantial durations, approximately 4.71 and 3.8 years, respectively, after which they progressively decrease and approach zero by the end of the five-year time horizon. The sustained, concurrent application of these controls highlights the importance of integrated, long-term public health programs that simultaneously manage HIV and mitigate environmental TB transmission to protect vulnerable populations effectively. From a public health implementation perspective, these results emphasize the need for early and continuous ART coverage combined with long-term environmental sanitation and infection control measures to reduce tuberculosis susceptibility among people living with HIV.

5.1.4. *Implementation of all controls (Strategy D)*

This comprehensive strategy integrates clinical treatment for both TB ($u_1(t)$) and HIV ($u_2(t)$) with environmental hygiene and sanitation ($u_3(t)$), creating a multi-faceted approach to enhance outcomes in high-burden, high-transmission settings. As depicted in Fig. 8(a) and 8(b), the implementation of this combined intervention leads to a significant and rapid reduction in both latent and active co-infected cases, with the model indicating a high probability of bringing the co-epidemic under control within approximately 2.5 years. To achieve this reduction in infectious classes cost-effectively, the optimal control profiles in Fig. 8(c) prescribe sustained maximal effort: TB therapy and HIV treatment are maintained at 100% for nearly 3 and 3.5 years, respectively, while environmental hygiene and sanitation is applied at full intensity for about 1.9 years, after which all controls gradually decline to zero by the fifth year. These profiles suggest a critical, intensive initial phase of 2 – 3.5 years is required for integrated programs, where clinical care must be prioritized for the longest duration, complemented by a shorter, targeted burst of environmental intervention to quickly break transmission cycles in vulnerable communities. Operationally, this strategy indicates that the greatest and most sustainable reduction in HIV–TB co-infection is achieved through coordinated implementation of TB case management, uninterrupted HIV treatment, and persistent environmental hygiene interventions, supporting integrated, multisectoral public health programming.

A comparative analysis of Strategies A through D reveals distinct differences in their efficacy at reducing HIV, TB, and co-infection prevalence, as well as environmental bacterial load. Among these, Strategy D, integrating TB treatment, HIV treatment, and environmental hygiene and sanitation, demonstrates the most rapid and comprehensive disease suppression, driving all infectious classes toward zero within approximately 2.4 years. This emphasizes the synergistic advantage of a fully integrated intervention. Strategy B, which excludes HIV treatment, effectively eliminates environmental bacteria and controls HIV–TB co-infection but proves less efficient in managing HIV-only cases. Conversely, Strategy C, implemented without TB-specific therapy, succeeds in reducing HIV incidence and environmental contamination, though the lack of direct TB intervention delays complete disease eradication. Strategy A, omitting environmental hygiene and sanitation, results in persistent environmental bacterial presence despite effective clinical treatment of human infections, highlighting the critical role of environmental hygiene and sanitation in achieving long-term control. Collectively, these findings indicate that while targeted strategies can achieve partial reductions in disease burden, a comprehensive, multi-faceted approach offers the most effective pathway toward sustained control and eventual eradication of HIV–TB co-infection. These results indicate that integrated implementation of TB case management, HIV treatment, and environmental sanitation offers the most robust and sustainable pathway for reducing HIV–TB co-infection in resource-limited settings.

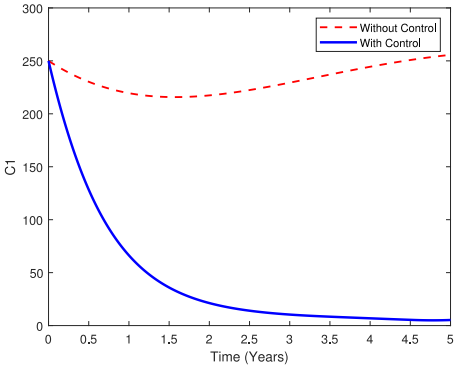

(a) Time evolution of HIV and latent TB co-infected individuals $C_1(t)$

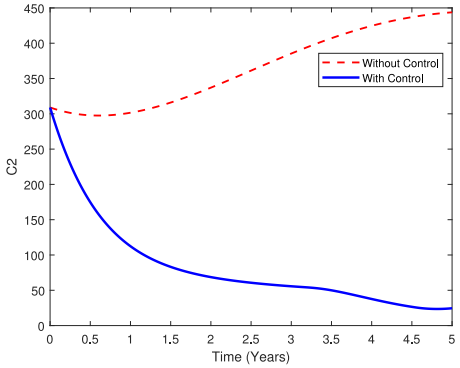

(b) Time evolution of HIV and active TB co-infected individuals $C_2(t)$

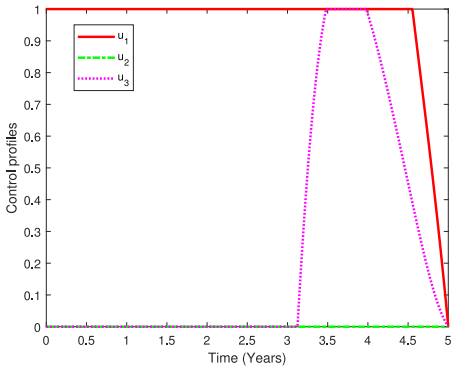

(c) Control profile

Fig. 6. Impact of combined TB treatment and environmental hygiene and sanitation (Strategy B) at $p = 0.982$.

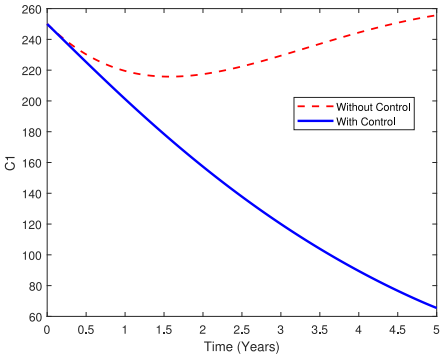

(a) Time evolution of HIV and latent TB co-infected individuals $C_1(t)$

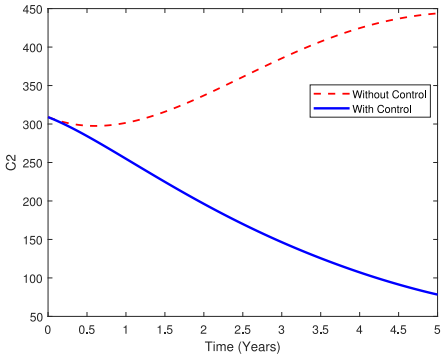

(b) Time evolution of HIV and active TB co-infected individuals $C_2(t)$

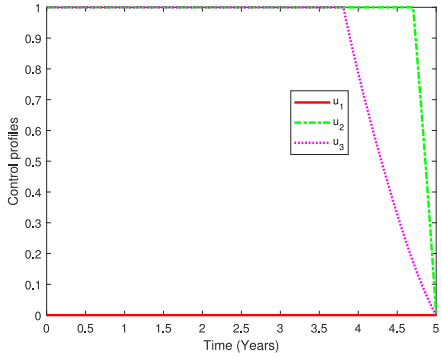

(c) Control profile

Fig. 7. Impact of combined HIV treatment and environmental hygiene and sanitation (Strategy C) at $p = 0.982$.

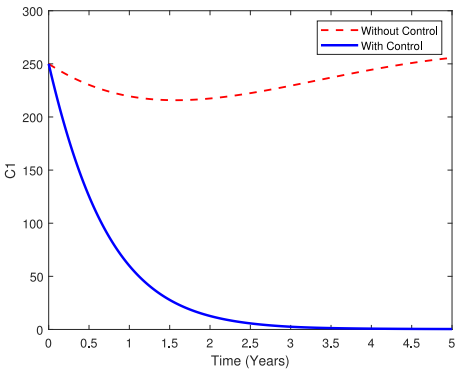

(a) Time evolution of HIV and latent TB co-infected individuals $C_1(t)$

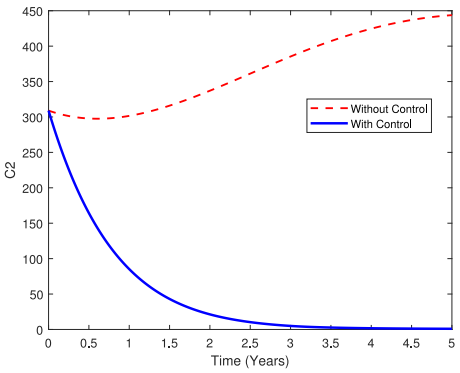

(b) Time evolution of HIV and active TB co-infected individuals $C_2(t)$

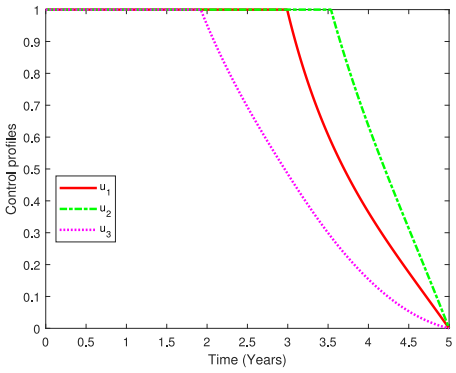

(c) Control profile

Fig. 8. Impact of integrated TB treatment, HIV treatment, and environmental hygiene and sanitation (Strategy D) at $p = 0.982$.

6. Conclusion

In this study, we formulated and analyzed a Caputo fractional-order model to investigate HIV–TB co-infection dynamics, explicitly incorporating environmental TB reservoirs and system memory effects. By integrating three time-dependent interventions: TB case-finding and treatment ($u_1(t)$), HIV treatment via ART ($u_2(t)$), and environmental hygiene and sanitation ($u_3(t)$), the model provides a comprehensive framework for evaluating the combined impact of clinical and environmental control strategies on disease transmission and persistence. The qualitative analysis confirmed the well-posedness of the system, including existence, uniqueness, positivity, and boundedness of solutions. Basic reproduction numbers, $\mathcal{R}_0^{TB}$ and $\mathcal{R}_0^{HIV}$, were derived, and the local stability of the disease-free equilibrium was assessed via the Routh–Hurwitz criterion. Furthermore, Ulam–Hyers stability was established, demonstrating the robustness of the fractional-order model under small perturbations.

Using reported HIV–TB co-infection data from Tanzania (2000–2023), the model parameters were estimated, yielding an excellent agreement between simulations and empirical observations and an optimal fractional order of $p = 0.982$. To assess the generalizability of the proposed framework, independent validation was conducted using epidemiological data from Kenya (2000–2023), where the model successfully reproduced observed trends without re-estimation of transmission parameters. This external validation demonstrates the robustness and transferability of the proposed fractional-order model across different high-burden settings.

A comparative analysis between the fractional-order model ($p = 0.982$) and the classical integer-order model ($p = 1$) revealed that the fractional formulation provides a more accurate and flexible representation of observed HIV–TB dynamics. Specifically, the fractional-order model better captured delayed treatment effects, prolonged disease persistence, and smoother epidemic trajectories, whereas the integer-order model tended to overestimate the speed of disease decline. These findings confirm that incorporating memory effects through fractional derivatives enhances model realism and improves alignment with epidemiological data.

Sensitivity analysis identified key parameters driving transmission dynamics, including treatment rates, environmental clearance, and transmission coefficients, highlighting the critical roles of sustained medical intervention and environmental control. Optimal control analysis revealed that among the four strategies considered, the fully integrated strategy combining TB treatment, HIV treatment, and environmental hygiene (Strategy D) produced the most rapid and sustained reduction in co-infection prevalence, driving infectious classes toward elimination within approximately 2.4 years. In contrast, strategies omitting environmental sanitation or either TB or HIV treatment resulted in delayed or incomplete disease control, underscoring the necessity of integrated, multi sectoral interventions.

From a public health perspective, these findings provide quantitative support for integrated HIV–TB control policies that simultaneously strengthen case detection, ensure uninterrupted treatment, and address environmental sources of transmission. Such coordinated approaches are particularly relevant for resource-limited, high-burden settings where environmental persistence of tuberculosis undermines purely clinical interventions.

Despite its contributions, this study has some limitations. The model assumes homogeneous mixing and does not explicitly account for spatial heterogeneity, stochastic variability, or behavioral factors that may influence transmission dynamics. Moreover, while control costs were incorporated, a full economic evaluation of intervention trade-offs was not performed. Future research will extend this framework to include spatially explicit and stochastic formulations, behavioral responses, and detailed cost-effectiveness analyses. Incorporating real time data

assimilation, climate and ventilation effects, and additional intervention layers such as vaccination and community-level behavioral change will further enhance the applicability of the model for evidence-based HIV–TB co-infection control planning.

CRediT authorship contribution statement

Dickson D. Luambano: Writing – original draft, Visualization, Methodology, Formal analysis, Conceptualization. **Mussa A. Stephano:** Writing – review & editing, Supervision, Methodology, Conceptualization. **Maranya M. Mayengo:** Writing – review & editing, Supervision, Methodology, Conceptualization.

Funding statement

No funding was received for this study.

Declaration of competing interest

The authors declare that they have no known competing financial interests or personal relationships that could have appeared to influence the work reported in this paper.

Appendix A. Proof of model well-posedness

This appendix provides the detailed proofs of the well-posedness results stated in Section 3.1.

A.1. Existence and uniqueness of solutions

Consider the fractional-order HIV–TB co-infection model (5) in the compact form

$$ {}_0^C D_t^p X(t) = Q(X(t)), \quad X(0) = X_0, $$

where $X(t) \in \mathbb{R}_+^{10}$ represents the state vector and $0 < p \leq 1$.

Proof. The mapping $Q : \mathbb{R}_+^{10} \to \mathbb{R}^{10}$ is continuous and satisfies a local Lipschitz condition with respect to X, as it is composed of polynomial and bilinear incidence terms with bounded coefficients. Therefore, according to standard results on Caputo fractional differential equations (Huo et al., 2015), the system admits a unique solution $X(t)$ on a finite interval $[0, T]$. □

A.2. Positivity of solutions

We show that solutions initiating in the non-negative orthant remain non-negative for all $t > 0$.

Proof. Let $X(0) \geq 0$. Consider the susceptible population equation. On the hyperplane $S = 0$,

$$ {}_0^C D_t^p S\Big|_{S=0} = \Omega^p > 0. $$

Hence, trajectories cannot cross into the negative region. Similarly, for each infected compartment x_i,

$$ {}_0^C D_t^p x_i\Big|_{x_i=0} \geq 0, $$

since all inflow terms are non-negative and all outflow terms vanish at the boundary. Therefore, by the generalized mean value theorem for fractional derivatives, solutions remain in $\mathbb{R}_+^{10}$ for all $t \geq 0$. □

A.3. Boundedness and positive invariant region

Proof. The analysis begins by recalling the Laplace transform of the Caputo derivative:

Definition 1. (Alshabanat et al., 2020): Laplace transform

$$ L\left\{ {}_0^C D_t^p (g(t))\right\} = s^p G(s) - \sum_{k=0}^{n-1} g^{(k)}(0) s^{p-k-1}. $$

To demonstrate boundedness and positive invariance of D, we analyze the total human population and environmental bacteria. Summing the human compartments yields:

$$ {}_0^C D_t^p N(t) = \Omega^p - \mu^p N(t). \tag{A.1} $$

Upon taking the Laplace transform on Eq. (A.1), we have

$$ s^p \tilde{N}(s) - s^{p-1} N(0) \leq \frac{\Omega^p}{s} - \mu^p \tilde{N}(s). \tag{A.2} $$

Solving the Eq. (A.2) for $\tilde{N}(s)$, we obtain

$$ \tilde{N}(s) \leq \frac{\Omega^p}{s(s^p + \mu^p)} + N(0)\frac{s^{p-1}}{s^p + \mu^p}. \tag{A.3} $$

Upon performing the inverse Laplace transform and considering the applicable bounds, Eq. (A.3) simplifies to:

$$ N(t) \leq \frac{\Omega^p}{\mu^p}. $$

Similarly, the dynamics of the environmental bacteria B are governed by:

$$ \begin{aligned} {}_0^C D_t^p B(t) &= k_1^p A + k_2^p C_2 - m^p B(t) \\ {}_0^C D_t^p B(t) &\leq (k_1^p + k_2^p) N(t) - m^p B(t). \end{aligned} \tag{A.4} $$

Using an analogous Laplace transform argument gives:

$$ B(t) \leq \frac{(k_1^p + k_2^p)\Omega^p}{\mu^p m^p}. \tag{A.5} $$

As all state variables remain non-negative and are bounded by these limits, the region D is positively invariant. Therefore, the model is both mathematically well-defined and consistent with epidemiological expectations. □

Appendix B. Derivation of basic reproduction number

The derivation follows the next-generation matrix framework proposed in Naik et al. (2020a) and adopted in Bolaji et al. (2024). The infected subsystems considered for this derivation are $x = \left(L, A, B, I, T_2, C_1, C_2, T_1\right)^T$, and let $b_1 = \mu^p + d_1^p + \tau^p, b_2 = m^p, b_3 = \mu^p + d_2^p + \eta^p, b_4 = \mu^p + d_2^p, b_5 = \mu^p + \theta_2^p + d_2^p + \tau_1^p, b_6 = \mu^p + d_3^p + \tau_2^p, b_7 = \mu^p + \eta^p + d_3^p, b_8 = \mu^p + \theta_1^p + \tau_0^p, b_9 = \eta^p, b_{10} = \tau_1^p, b_{11} = \tau_2^p$. Consequently, the vectors for new infections and transitions between compartments, respectively are defined as follows:

$$ \mathcal{F} = \begin{pmatrix} \chi_1^C S + \phi\chi_1^C R \\ 0 \\ 0 \\ \chi_2^C S + \chi_2^C R \\ 0 \\ 0 \\ 0 \\ 0 \end{pmatrix}, \quad \mathcal{V} = \begin{pmatrix} \left(b_8 + \chi_2^C\right) L \\ -\theta_1^p L + \left(b_1 + \chi_2^C\right) A \\ b_2 B - k_1^p A - k_2^p C_2 \\ \left(b_3 + \delta\chi_1^C\right) I \\ -b_9\left(I + T_1\right) + b_4 T_2 \\ -\chi_2^C L + b_5 C_1 \\ -\theta_2^p C_1 - \delta\chi_1^C I - \chi_2^C A + b_6 C_2 \\ -b_{10} C_1 - b_{11} C_2 + b_7 T_1 \end{pmatrix}, $$

By evaluating the Jacobian matrices $\mathbf{F} = D_x\mathcal{F}(x)$ and $\mathbf{V} = D_x\mathcal{V}(x)$ at the disease-free equilibrium, we derive

$$ \mathbf{F} = \begin{pmatrix} 0 & \beta_T^p & \frac{\beta_1^p \Omega^p}{\mu^p} & 0 & 0 & 0 & q_1\beta_T^p & 0 \\ 0 & 0 & 0 & 0 & 0 & 0 & 0 & 0 \\ 0 & 0 & 0 & \beta_H^p & 0 & q_2\beta_H^p & 0 & 0 \\ 0 & 0 & 0 & 0 & 0 & 0 & 0 & 0 \\ 0 & 0 & 0 & 0 & 0 & 0 & 0 & 0 \\ 0 & 0 & 0 & 0 & 0 & 0 & 0 & 0 \\ 0 & 0 & 0 & 0 & 0 & 0 & 0 & 0 \\ 0 & 0 & 0 & 0 & 0 & 0 & 0 & 0 \end{pmatrix}, $$

$$\mathbf{V} = \begin{pmatrix} b_8 & 0 & 0 & 0 & 0 & 0 & 0 & 0 \\ -\theta_1^p & b_1 & 0 & 0 & 0 & 0 & 0 & 0 \\ 0 & -k_1^p & b_2 & 0 & 0 & 0 & -k_2^p & 0 \\ 0 & 0 & 0 & b_3 & 0 & 0 & 0 & 0 \\ 0 & 0 & 0 & -b_9 & b_4 & 0 & 0 & -b_9 \\ 0 & 0 & 0 & 0 & 0 & b_5 & 0 & 0 \\ 0 & 0 & 0 & 0 & 0 & -\theta_2^p & b_6 & 0 \\ 0 & 0 & 0 & 0 & 0 & -b_{10} & -b_{11} & b_7 \end{pmatrix}$$

The next-generation matrix is given by

$$\mathcal{K} = \mathbf{F}\mathbf{V}^{-1}.$$

The basic reproduction number is defined as

$$\mathcal{R}_0 = \rho(\mathcal{K}),$$

where $\rho(\cdot)$ denotes the spectral radius. Due to block diagonality in $\mathbf{V}$, $\mathcal{K}$ simplifies yielding two independent basic reproduction numbers. Since the diseases are independent at the DFE, the basic reproduction number is given by

$$\mathcal{R}_0 = \max\left\{\mathcal{R}_0^{TB}, \mathcal{R}_0^{HIV}\right\} \tag{B.1}$$

with expressions given in Section 3.2.

Appendix C. Proof of Theorem 3

Proof. The Jacobian matrix $J(E^0)$ is constructed by taking the partial derivatives of system (A.2) with respect to the state variables $S(t), L(t), A(t), R(t), B(t), I(t), T_2(t), C_1(t), C_2(t), T_1(t)$ and evaluating them at E^0. The resulting matrix is expressed as:

$$J(E^0) = \begin{pmatrix} -\mu^p & 0 & -G_6 & 0 & -G_7 & -G_8 & 0 & -q_2G_8 & -q_1G_6 & 0 \\ 0 & -G_1 & G_6 & 0 & G_7 & 0 & 0 & 0 & q_1G_6 & 0 \\ 0 & \theta_1^p & -G_2 & 0 & 0 & 0 & 0 & 0 & G_8 & 0 \\ 0 & \tau_0^p & \tau_0^p & -\mu^p & 0 & 0 & 0 & 0 & 0 & 0 \\ 0 & 0 & k_1^p & 0 & -m^p & 0 & 0 & 0 & k_2^p & 0 \\ 0 & 0 & 0 & 0 & 0 & -G_3 & 0 & q_2G_8 & 0 & 0 \\ 0 & 0 & 0 & 0 & 0 & G_9 & -(\mu^p + d_2^p) & 0 & 0 & G_9 \\ 0 & 0 & 0 & 0 & 0 & 0 & 0 & -G_5 & 0 & 0 \\ 0 & 0 & 0 & 0 & 0 & 0 & 0 & \theta_2^p & -G_4 & 0 \\ 0 & 0 & 0 & 0 & 0 & 0 & 0 & G_{10} & G_{11} & -G_3 \end{pmatrix}$$

where, $G_1 = \mu^p + \theta_1^p + \tau_0^p, G_2 = \mu^p + d_1^p + \tau^p, G_3 = \mu^p + d_2^p + \eta^p, G_4 = \mu^p + \theta_2^p + d_2^p + \tau_1^p, G_5 = \mu^p + d_3^p + \tau_2^p, G_6 = \beta_T^p, G_7 = \beta_1\dfrac{\Omega^p}{\mu^p}, G_8 = \beta_H^p, G_9 = \eta^p, G_{10} = \tau_1^p, G_{11} = \tau_2^p$. Solving the characteristic equation $\det(J(E^0) - \lambda I) = 0$ provides the eigenvalues.

$$\lambda_1 = -\mu^p, \lambda_2 = -\mu^p, \lambda_3 = -(\mu^p + d_2^p), \lambda_4 = -G_3, \lambda_5 = -G_3.$$

To compute the remaining eigenvalues, the submatrix P is considered, and it is defined as:

$$P = \begin{pmatrix} -G_1 & G_6 & G_7 & 0 & q_1G_6 \\ \theta_1^p & -G_2 & 0 & 0 & G_8 \\ 0 & k_1^p & -m^p & 0 & k_2 \\ 0 & 0 & 0 & -G_5 & 0 \\ 0 & 0 & 0 & \theta_2^p & -G_4 \end{pmatrix}$$

The matrix P yields the following characteristic polynomial:

$$P(\lambda) = \lambda^5 + a_1\lambda^4 + a_2\lambda^3 + a_3\lambda^2 + a_4\lambda + a_5 \tag{C.1}$$

with the coefficients

$$\begin{aligned} a_1 &= G_1 + G_2 + G_4 + G_5 + m^p, \\ a_2 &= G_1G_2 + G_1G_4 + G_1G_5 + G_1m^p + G_2G_4 + G_2G_5 + G_2m^p + G_4G_5 \\ &\quad + G_4m^p + G_5m^p - \theta_1^pG_6, \\ a_3 &= -G_7\theta_1^pk_1^p + G_1G_2G_4 + G_1G_2G_5 + G_1G_2m^p + G_1G_4G_5 + G_1G_4m^p \\ &\quad + G_1G_5m^p + G_2G_4G_5 + G_2G_4m^p + G_2G_5m^p + G_4G_5m^p \\ &\quad - G_4G_6\theta_1^p - G_5G_6\theta_1^p - G_6\theta_1^pm^p, \\ a_4 &= -G_7G_4\theta_1^pk_1^p - G_7G_5\theta_1^pk_1^p + G_1G_2G_4G_5 + G_1G_2G_4m^p + G_1G_2G_5m^p \\ &\quad + G_1G_4G_5m^p + G_2G_4G_5m^p - G_4G_5G_6\theta_1^p - G_4G_6\theta_1^pm^p - G_5G_6\theta_1^pm^p, \\ a_5 &= -G_7G_4G_5\theta_1^pk_1^p + G_1G_2G_4G_5m^p - G_4G_5G_6\theta_1^pm^p. \end{aligned}$$

The Hurwitz principal leading minors D_n (upper-left $n\times n$ determinants of the Hurwitz matrix) for the polynomial $\lambda^5+a_1\lambda^4+a_2\lambda^3+a_3\lambda^2+a_4\lambda+a_5$ are given by the well-known formulas:

$$D_1 = a_1,$$

$$D_2 = \det\begin{pmatrix} a_1 & a_3 \\ 1 & a_2 \end{pmatrix} = a_1a_2 - a_3,$$

$$D_3 = \det\begin{pmatrix} a_1 & a_3 & a_5 \\ 1 & a_2 & a_4 \\ 0 & a_1 & a_3 \end{pmatrix} = -a_1^2a_4 + a_1a_2a_3 + a_1a_5 - a_3^2,$$

$$\begin{aligned} D_4 &= \det\begin{pmatrix} a_1 & a_3 & a_5 & 0 \\ 1 & a_2 & a_4 & 0 \\ 0 & a_1 & a_3 & a_5 \\ 0 & 1 & a_2 & a_4 \end{pmatrix} \\ &= -a_1^2a_4^2 - a_1a_2^2a_5 + a_1a_2a_3a_4 + 2a_1a_4a_5 + a_2a_3a_5 - a_3^2a_4 - a_5^2, \end{aligned}$$

$D_5 = \det(H) = a_5\,D_4$ (equivalently, the full Hurwitz determinant).

According to the Routh–Hurwitz criterion (DeJesus and Kaufman, 1987; Morris, 1962), the equilibrium is locally asymptotically stable if and only if all eigenvalues of P have negative real parts. This condition holds when

$$a_1 > 0,\ a_2 > 0,\ a_3 > 0,\ a_4 > 0,\ a_5 > 0, \tag{C.2}$$

and

$$D_1 > 0,\ D_2 > 0,\ D_3 > 0,\ D_4 > 0,\ D_5 > 0. \tag{C.3}$$

It is evident that $D_1 = a_1 > 0$, since $G_1 + G_2 + G_4 + G_5 + m^p + u_4 > 0$, and $D_2 > 0$ if $a_1a_2 > a_3$, while $D_3 > 0$ if $a_1a_2a_3 + a_1a_5 > a_1^2a_4 + a_3^2$. Also $D_4 > 0$ if

$$a_1a_2a_3a_4 + 2a_1a_4a_5 + a_2a_3a_5 > a_1^2a_4^2 + a_1a_2^2a_5 + a_3^2a_4 + a_5^2$$

Similarly, $D_5 > 0$ if

$$a_1a_2a_3a_4a_5 + 2a_1a_4a_5^2 + a_2a_3a_5^2 > a_1^2a_4^2a_5 + a_1a_2^2a_5^2 + a_3^2a_4a_5 + a_5^3$$

Hence, if all the Routh–Hurwitz conditions are satisfied, it results in

$$|\arg(\lambda_i)| > \frac{\pi p}{2}, \quad i = 1, \ldots, 10.$$

Accordingly, the disease-free equilibrium of the HIV–TB co-infection model is locally asymptotically stable. □

Appendix D. Ulam–Hyers stability analysis

This appendix provides the detailed proof of Ulam–Hyers stability stated in Section 3.4.

D.1. Preliminaries

Consider the perturbed system

$${}_0^C D_t^p X(t) = \mathcal{Q}(X(t)) + \varepsilon(t),$$

where $\|\varepsilon(t)\| \le \epsilon$.

D.2. Ulam–Hyers stability definition

The system is said to be Ulam–Hyers stable if there exists a constant $C > 0$ such that

$$\|X(t) - \tilde{X}(t)\| \le C\epsilon,$$

for all $t \in [0, T]$, where $X(t)$ is the exact solution and $\tilde{X}(t)$ is an approximate solution.

D.3. Proof of Ulam–Hyers stability

Proof. Using the integral representation of the Caputo derivative,

$$X(t)-\tilde{X}(t)=\frac{1}{\Gamma(p)}\int_0^t(t-\tau)^{p-1}\left[\mathcal{Q}(X(\tau))-\mathcal{Q}(\tilde{X}(\tau))\right]d\tau+\mathcal{O}(\epsilon).$$

Since $\mathcal{Q}$ is Lipschitz continuous with constant κ,

$$\|X(t)-\tilde{X}(t)\|\le\frac{\kappa}{\Gamma(p)}\int_0^t(t-\tau)^{p-1}\|X(t)-\tilde{X}(t)\|\,d\tau+\epsilon. \tag{D.1}$$

Applying a generalized Grönwall inequality for fractional integrals yields

$$\|X(t)-\tilde{X}(t)\|\le\frac{\Gamma(p+1)}{\Gamma(p+1)-\kappa T^p}\epsilon,$$

provided that

$$\Gamma(p+1)>\kappa T^p.$$

Hence, Therefore, the fractional model (5) is Ulam–Hyers stable on $[0,T]$. □

Appendix E. Derivation of the effective reproduction number for the controlled system

This appendix provides a detailed derivation of the effective reproduction number $\mathcal{R}_e$ for the HIV–TB co-infection model with time-dependent control interventions, as introduced in Section 4.1 of the main text. The derivation follows the next-generation matrix approach (Naik et al., 2020a; Bolaji et al., 2024), extended to incorporate the control variables $u_1(t)$, $u_2(t)$, and $u_3(t)$. For the controlled system, the new infections and transitions are:

$$\mathcal{F}_i=\begin{pmatrix}\chi_1^C S+\phi\chi_1^C R\\0\\0\\\chi_2^C S+\chi_2^C R\\0\\0\\0\\0\end{pmatrix},\quad \mathcal{V}_i=\begin{pmatrix}\left(\mu^p+\theta_1^p+\tau_0^p+u_1+\chi_2^C\right)L\\-\theta_1^pL+\left(\mu^p+d_1^p+\tau^p+u_1+\chi_2^C\right)A\\(m^p+u_3)B-k_1^pA-k_2^pC_2\\\left(\mu^p+d_2^p+\eta^p+u_2+\delta\chi_1^C\right)I\\-(\eta^p+u_2)I-(\eta^p+u_2)T_1+(\mu^p+d_2^p)T_2\\-\chi_2^CL+(\mu^p+d_2^p+\theta_2^p+\tau_1^p+u_1)C_1\\-\theta_2^pC_1-\delta\chi_1^CI-\chi_2^CA+(\mu^p+d_3^p+\tau_2^p+u_1)C_2\\-(\tau_1^p+u_1)C_1-(\tau_2^p+u_1)C_2+(\mu^p+d_3^p+\eta^p+u_2)T_1\end{pmatrix},$$

We linearize the system at the disease-free equilibrium E^0 and construct the matrices $\mathbf{F}$ and $\mathbf{V}$ accordingly.

$$\mathbf{F}=\left[\frac{\partial\mathcal{F}_i}{\partial x_j}\right]_{E^0},\quad \mathbf{V}=\left[\frac{\partial\mathcal{V}_i}{\partial x_j}\right]_{E^0},$$

with $\mathcal{F}_i$ and $\mathcal{V}_i$ representing new infection and transition terms, respectively. Therefore,

$$\mathbf{F}=\begin{pmatrix}0&\beta_T^p&\frac{\beta_1^p\Omega^p}{\mu^p}&0&0&0&q_1\beta_T^p&0\\0&0&0&0&0&0&0&0\\0&0&0&\beta_H^p&0&q_2\beta_H^p&0&0\\0&0&0&0&0&0&0&0\\0&0&0&0&0&0&0&0\\0&0&0&0&0&0&0&0\\0&0&0&0&0&0&0&0\\0&0&0&0&0&0&0&0\end{pmatrix},$$

$$\mathbf{V}=\begin{pmatrix}a_1&0&0&0&0&0&0&0\\-\theta_1^p&a_2&0&0&0&0&0&0\\0&-k_1^p&a_3&0&0&0&-k_2^p&0\\0&0&0&a_4&0&0&0&0\\0&0&0&-a_5&a_6&0&0&-a_5\\0&0&0&0&0&a_7&0&0\\0&0&0&0&0&-\theta_2^p&a_8&0\\0&0&0&0&0&-a_9&-a_{10}&a_{11}\end{pmatrix}$$

where $a_1=\mu^p+\theta_1^p+\tau_0^p+u_1$, $a_2=\mu^p+d_1^p+\tau^p+u_1$, $a_3=m^p+u_3$, $a_4=\mu^p+d_2^p+\eta^p+u_2$, $a_5=\eta^p+u_2$, $a_6=\mu^p+d_2^p$, $a_7=\mu^p+d_2^p+\theta_2^p+\tau_1^p+u_1$, $a_8=\mu^p+d_3^p+\tau_2^p+u_1$, $a_9=\tau_1^p+u_1$, $a_{10}=\tau_2^p+u_1$, and $a_{11}=\mu^p+d_3^p+\eta^p+u_2$. The next-generation matrix is defined as

$$\mathbf{K}=\mathbf{F}\mathbf{V}^{-1}.$$

Since $\mathbf{K}$ is block diagonal at the disease-free equilibrium, its spectrum decomposes into independent TB and HIV components.

TB subsystem. The TB subsystem consists of the compartments (L,A,B,C_2). The corresponding new infection and transition matrices are given by

$$\mathbf{F}_{TB}=\begin{pmatrix}0&\beta_T^p&\beta_1^pS_0&q_1\beta_T^p\\0&0&0&0\\0&0&0&0\\0&0&0&0\end{pmatrix},\qquad \mathbf{V}_{TB}=\begin{pmatrix}a_1&0&0&0\\-\theta_1^p&a_2&0&0\\0&-k_1^p&a_3&0\\0&-k_2^p&0&a_7\end{pmatrix}.$$

Computing $\mathbf{V}_{TB}^{-1}$ and forming the next-generation matrix

$$\mathbf{K}_{TB}=\mathbf{F}_{TB}\mathbf{V}_{TB}^{-1},$$

the effective reproduction number for the TB subsystem is obtained as the spectral radius of $\mathbf{K}_{TB}$, yielding

$$\mathcal{R}_e^{TB}=\frac{\theta_1^p\left(\Omega^p\beta_1^pk_1^p+\beta_1^pm^p\mu^p+\beta_1^p\mu^pu_3\right)}{\mu^pa_1a_2a_3}.$$

Substituting the expressions for a_1, a_2, and a_3 into the above equation yields Eq. (15) in the main text.

HIV subsystem. The HIV subsystem consists of the compartments (I,C_1). The corresponding new infection and transition matrices are given by

$$\mathbf{F}_{HIV}=\begin{pmatrix}\beta_H^p&q_2\beta_H^p\\0&0\end{pmatrix},\qquad \mathbf{V}_{HIV}=\begin{pmatrix}a_4&0\\0&a_5\end{pmatrix}.$$

The next-generation matrix is

$$\mathbf{K}_{HIV}=\mathbf{F}_{HIV}\mathbf{V}_{HIV}^{-1}.$$

The effective reproduction number for the HIV subsystem is therefore given by the spectral radius of $\mathbf{K}_{HIV}$, yielding

$$\mathcal{R}_e^{HIV}=\frac{\beta_H^p}{a_4}=\frac{\beta_H^p}{\mu^p+d_2^p+\eta^p+u_2}.$$

This expression corresponds to Eq. (16) in the main text. Since the diseases are independent at the disease-free equilibrium, the overall effective reproduction number is given by

$$\mathcal{R}_e=\max\left\{\mathcal{R}_e^{TB},\mathcal{R}_e^{HIV}\right\}. \tag{E.1}$$

This completes the derivation of the effective reproduction number for the controlled HIV–TB co-infection model.

Data availability

Data will be made available on request.

References

Abdullahi, O.A., Ngari, M.M., Sanga, D., Katana, G., Willetts, A., 2019. Mortality during treatment for tuberculosis; a review of surveillance data in a rural county in Kenya. PLoS One 14 (7), e0219191.

Adesola, O.I., Temilade, M.I., Emmanuel, P.M., Oladele, A.S., Adeyemi, A.G., Sunday, S., Olumuyiwa, A.S., 2024. Mathematical analysis of optimal control of human immunodeficiency virus (HIV) co-infection with tuberculosis (TB). Asian Res. J. Curr. Sci. 23–53.

Adeyemo, S., Sangotola, A., Korosteleva, O., 2023. Modeling transmission dynamics of tuberculosis-HIV co-infection in South Africa. Epidemiologia 4 (4), 408–419. http://dx.doi.org/10.3390/epidemiologia4040036.

Aggarwal, R., Raj, Y.A., 2021. A fractional order HIV-TB co-infection model in the presence of exogenous reinfection and recurrent TB. Nonlinear Dynam. 104, 4701–4725. http://dx.doi.org/10.1007/s11071-020-06232-x.

Alqudah, M.A., Shah, K., Mofarreh, F., Abdeljawad, T., 2026. Mathematical modeling of psychological disease by using artificial intelligence tools. Fractals 34 (1), 2550101.
Alshabanat, A., Jleli, M., Kumar, S., Samet, B., 2020. Generalization of Caputo-Fabrizio fractional derivative and applications to electrical circuits. Front. Phys. 8, 64.
Angstmann, C.N., Henry, B.I., McGann, A.V., 2016. A fractional-order infectivity SIR model. Phys. A 452, 86–93.
Awoke, T.D., Kassa, S.M., 2018. Optimal control strategy for TB-HIV/AIDS co-infection model in the presence of behaviour modification. Processes 6 (5), 48. http://dx.doi.org/10.3390/pr6050048.
Ayele, T.K., Doungmo Goufo, E.F., Mugisha, S., 2024a. Co-infection mathematical model for HIV/AIDS and tuberculosis with optimal control in Ethiopia. PLOS ONE 19 (12), e0312539. http://dx.doi.org/10.1371/journal.pone.0312539.
Ayele, T.K., Doungmo Goufo, E.F., Mugisha, S., 2024b. Mathematical modeling of tuberculosis with drug resistance in the presence of optimal control: A case study in ethiopia. J. Biol. Systems 32 (04), 1541–1585.
Ayele, T.K., Goufo, E.F.D., Mugisha, S., 2021. Mathematical modeling of HIV/AIDS with optimal control: a case study in ethiopia. Results Phys. 26, 104263.
Bolaji, B., Onoja, T., Benedict, A.C., Omede, B.I., Odionyenma, U.B., 2024. Dynamical analysis of HIV-TB co-infection transmission model in the presence of treatment for TB. Bull. Biomath. 2 (1), 21–56. http://dx.doi.org/10.59292/bulletinbiomath.2024002.
Chinyoka, M., Gashirai, T.B., Mushayabasa, S., 2021. On the dynamics of a fractional-order Ebola epidemic model with nonlinear incidence rates. Discrete Dyn. Nat. Soc. 2021 (1), 2125061. http://dx.doi.org/10.1155/2021/2125061.
Chitnis, N., Hyman, J.M., Cushing, J.M., 2008. Determining important parameters in the spread of malaria through the sensitivity analysis of a mathematical model. Bull. Math. Biol. 70, 1272–1296. http://dx.doi.org/10.1007/s11538-008-9299-0.
DeJesus, E.X., Kaufman, C., 1987. Routh-Hurwitz criterion in the examination of eigenvalues of a system of nonlinear ordinary differential equations. Phys. Rev. A 35 (12), 5288.
Devi, A.S., Naik, P.A., Boulaaras, S., Sene, N., Huang, Z., 2025. Understanding the transmission mechanism of HIV/TB co-infection using fractional framework with optimal control. Int. J. Numer. Modelling, Electron. Netw. Devices Fields 38 (4), e70097.
Edward, S., 2024. A fractional order model for the transmission dynamics of shigellosis. Heliyon 10 (10).
Endalamaw, A., Ambachew, S., Geremew, D., Habtewold, T., 2019. HIV infection and unknown HIV status among tuberculosis patients in ethiopia: a systematic review and meta-analysis. Int. J. Tuberc. Lung Dis. 23 (2), 187–194.
Farman, M., Usman, M., Ahmad, A., Ahmad, M., 2020. Mathematical analysis of fractional order co-infection TB and HIV model. Int. J. Anal. Appl. 18 (1), 16–32.
Gao, C., Zhang, T., Liao, Y., Wang, Y., Jiao, H., Wu, M., Cui, Q., Wang, K., Wang, L., 2024. Modelling of tuberculosis dynamics incorporating indirect transmission of contaminated environment and infectivity of smear-negative individuals: A case study for Xinjiang, China. Acta Trop. 254, 107130. http://dx.doi.org/10.1016/j.actatropica.2024.107130.
Gelaw, Y., Williams, G., Soares Magalhaes, R.J., Gilks, C.F., Assefa, Y., 2019. HIV prevalence among tuberculosis patients in sub-Saharan Africa: a systematic review and meta-analysis. AIDS Behav. 23, 1561–1575.
Gemeda, A.E., Obsu, L.L., Gurmu, E.D., Degefa, S.T., 2025. Fractional order modeling of HIV/AIDS and TB co-infection with vaccination and treatment therapies. Comput. Math. Model. 1–40.
Huo, J., Zhao, H., Zhu, L., 2015. The effect of vaccines on backward bifurcation in a fractional order HIV model. Nonlinear Anal. Real World Appl. 26, 289–305. http://dx.doi.org/10.1016/j.nonrwa.2015.03.009.
Karim, M., Kouidere, A., Rachik, M., Shah, K., Abdeljawad, T., 2023. Inverse problem to elaborate and control the spread of COVID-19: A case study from Morocco. AIMS Math. 8 (10), 23500–23518.
Khan, M.A., Ullah, S., Kumar, S., 2021. A robust study on 2019-nCOV outbreaks through non-singular derivative. Eur. Phys. J. Plus 136 (2), 168.
Kheiri, H., Jafari, M., 2018. Optimal control of a fractional-order model for the HIV/AIDS epidemic. Int. J. Biomath. 11 (07), 1850086. http://dx.doi.org/10.1142/S1793524518500869.
Kilale, A.M., Pantoja, A., Jani, B., Range, N., Ngowi, B.J., Makasi, C., Majaha, M., Manga, C.D., Haule, S., Wilfred, A., et al., 2022. Economic burden of tuberculosis in tanzania: a national survey of costs faced by tuberculosis-affected households. BMC Public Health 22 (1), 600.
Kumar, S., Chauhan, R.P., Momani, S., Hadid, S., 2024. Numerical investigations on COVID-19 model through singular and non-singular fractional operators. Numer. Methods Partial Differential Equations 40 (1), e22707.
Kumar, S., Kumar, R., Momani, S., Hadid, S., 2023. A study on fractional COVID-19 disease model by using Hermite wavelets. Math. Methods Appl. Sci. 46 (7), 7671–7687.
Kumar, S., Kumar, A., Samet, B., Dutta, H., 2021. A study on fractional host-parasitoid population dynamical model to describe insect species. Numer. Methods Partial Differential Equations 37 (2), 1673–1692.
Lenhart, S., Workman, J.T., 2007. Optimal Control Applied to Biological Models. Chapman and Hall /CRC.
Li, Q., Wang, F., 2023. An epidemiological model for tuberculosis considering environmental transmission and reinfection. Mathematics 11 (11), 2423.
Liu, Y., Gao, S., Chen, D., Liu, B., 2024. Modeling the transmission dynamics and optimal control strategy for huanglongbing. Mathematics 12 (17), 2648.
Lusekelo, E., Helikumi, M., Kuznetsov, D., Mushayabasa, S., 2023. Dynamic modelling and optimal control analysis of a fractional order chikungunya disease model with temperature effects. Results Control. Optim. 10, 100206. http://dx.doi.org/10.1016/j.rico.2023.100206.
Mallela, A., Lenhart, S., Vaidya, N.K., 2016. HIV-TB co-infection treatment: Modeling and optimal control theory perspectives. J. Comput. Appl. Math. 307, 143–161.
McAsey, M., Mou, L., Han, W., 2012. Convergence of the forward-backward sweep method in optimal control. Comput. Optim. Appl. 53, 207–226. http://dx.doi.org/10.1007/s10589-011-9454-7.
McBain, R.K., Jordan, M., Mann, C., Ruhago, G.M., Lee, B., Forsythe, S., Stewart, K., Brown, J., Nandakumar, A., 2023. National evaluation of HIV service resource allocation in Tanzania. AIDS Behav. 27 (10), 3498–3507.
Mchunu, G., Van Griensven, J., Hinderaker, S., Kizito, W., Sikhondze, W., Manzi, M., Dlamini, T., Harries, A., 2016. High mortality in tuberculosis patients despite HIV interventions in swaziland. Public Health Action 6 (2), 105–110.
Morris, J., 1962. The routh and Routh-Hurwitz stability criteria: Their derivation by a novel method using comparatively elementary algebra. Aircr. Eng. Aerosp. Technol. 34 (1), 25–27.
Naik, P.A., Yavuz, M., Qureshi, S., Zu, J., Townley, S., 2020a. Modeling and analysis of COVID-19 epidemics with treatment in fractional derivatives using real data from Pakistan. Eur. Phys. J. Plus 135, 1–42. http://dx.doi.org/10.1140/epjp/s13360-020-00840-9.
Naik, P.A., Zu, J., Owolabi, K.M., 2020b. Global dynamics of a fractional order model for the transmission of HIV epidemic with optimal control. Chaos Solitons Fractals 138, 109826.
Obeagu, E.I., Obeagu, G.U., 2023. Human immunodeficiency virus and tuberculosis infection: A review of prevalence of associated factors. Int. J. Adv. Multidiscip. Res 10 (10), 56–62. http://dx.doi.org/10.22192/ijamr.2023.10.10.005.
Okyere, E., Olaniyi, S., Bonyah, E., 2020. Analysis of Zika virus dynamics with sexual transmission route using multiple optimal controls. Sci. Afr. 9, e00532.
Olaniyi, S., Gbadamosi, B., Olopade, I., 2013. A nonlinear deterministic model for HIV infection dynamics with optimal control strategy using power series method. J. Nigerian Math. Soc. 32 (1–3), 87–95.
Pathmanathan, I., Pasipamire, M., Pals, S., Dokubo, E.K., Preko, P., Ao, T., Mazibuko, S., Ongole, J., Dhlamini, T., Haumba, S., 2018. High uptake of antiretroviral therapy among HIV-positive TB patients receiving co-located services in Swaziland. PLoS One 13 (5), e0196831.
Pinto, C.M., Carvalho, A.R., 2017. A latency fractional order model for HIV dynamics. J. Comput. Appl. Math. 312, 240–256.
Pontryagin, L.S., 2018. Mathematical Theory of Optimal Processes. Routledge.
Raza, N., Irum, S., Niazai, S., Ullah, M.A., Alshahrani, M.Y., Omame, A., 2025. A mathematical framework of HIV and TB co-infection dynamics. Sci. Rep. 15 (1), 11465. http://dx.doi.org/10.1038/s41598-025-11465.
Ruoja, C.S., Nyerere, N., Mayengo, M.M., Nyabadza, F., 2025. Dynamic and optimal control of TB transmission: the role of vaccination funding and social processes using Caputo-type framework. Int. J. Dyn. Control. 13 (12), 414.
Seidu, B., Makinde, O.D., Seini, I.Y., 2023. On the optimal control of HIV-TB co-infection and improvement of workplace productivity. Discrete Dyn. Nat. Soc. 2023 (1), 3716235. http://dx.doi.org/10.1155/2023/3716235.
Shah, K., Ahmad, S., Ullah, A., Abdeljawad, T., 2024. Study of chronic myeloid leukemia with T-cell under fractal-fractional order model. Open Phys. 22 (1), 20240032.
Shah, K., Rehman, K.U., Abdalla, B., Abdeljawad, T., Shatanawi, W., 2025a. Using neural network and fractals fractional analysis to predict the eye disease infection caused by conjunctivitis virus. Fractals 2540204.
Shah, K., Sarwar, M., Abdeljawad, T., et al., 2025b. Study of fractional order epidemic compartmental model by using artificial deep neural networks. Neural Netw. 107944.
Sher, M., Shah, K., Ali, Z., Abdeljawad, T., Alqudah, M., 2025. Using deep neural network in computational analysis of coupled systems of fractional integro-differential equations. J. Comput. Appl. Math. 116912.
Sinan, M., Ali, A., Shah, K., Assiri, T.A., Nofal, T.A., 2021. Stability analysis and optimal control of Covid-19 pandemic SEIQR fractional mathematical model with harmonic mean type incidence rate and treatment. Results Phys. 22, 103873.
Singh, R., Ali, S., Jain, M., et al., 2016. Epidemic model of HIV/AIDS transmission dynamics with different latent stages based on treatment. Am. J. Appl. Math 4, 222–234.
Stephano, M.A., Mayengo, M.M., Irunde, J.I., 2024. The role of asymptomatic carriers on the dynamics of a lymphatic filariasis model incorporating control strategies. Results Control. Optim. 15, 100425.
Teklu, S.W., Abebaw, Y.F., Terefe, B.B., Mamo, D.K., 2023. HIV/AIDS and TB co-infection deterministic model bifurcation and optimal control analysis. Informatics Med. Unlocked 41, 101328. http://dx.doi.org/10.1016/j.imu.2023.101328.
Ullah, A., Sakidin, H., Gul, S., Alharthi, T.N., Metwally, D.S., Hamed, Y., Shah, K., Sambas, A., 2025. Exploring the effectiveness of an optimal control model for Marijuana consumption. Eur. J. Pure Appl. Math. 18 (3), 6451–6451.
West, R.W., Thompson, J.R., 1997. Modeling the impact of HIV on the spread of tuberculosis in the united states. Math. Biosci. 143 (1), 35–60.

World Health Organization, 2023a. Global tuberculosis programme data,2023. https://www.who.int/teams/global-tuberculosis-programme/data. (Accessed 10 April 2025).
World Health Organization, 2023b. Life expectancy, united Republic of tanzania, 2023. https://data.who.int/countries/834. (Accessed 10 April 2025).
World Health Organization, 2023c. Life expectancy,Republic of Kenya, 2023. https://data.who.int/countries/404. (Accessed 3 February 2026).
World Health Organization (WHO), 2023. Global tuberculosis report 2023. URL https://www.who.int/publications/i/item/9789240083851. Accessed: 2024-04-04.
Zahli, R., Zeroual, K., Fatmi, N.I., 2024. Tuberculosis and HIV/AIDS co-dynamics: A mathematical model and sensitivity analysis. Commun. Math. Biol Neurosci. 2024.